Document downloaded from:

http://hdl.handle.net/10251/183795

This paper must be cited as:

Serrano, J.; Arnau Martínez, FJ.; García-Cuevas González, LM.; Farias, VH. (2021). Oxy-fuel combustion feasibility of compression ignition engines using oxygen separation membranes for enabling carbon dioxide capture. Energy Conversion and Management. 247:1-17. https://doi.org/10.1016/j.enconman.2021.114732

The final publication is available at

https://doi.org/10.1016/j.enconman.2021.114732

Copyright Elsevier

Additional Information

Oxy-fuel combustion feasibility of compression ignition engines using oxygen separation membranes for enabling carbon dioxide capture

J.R. Serrano, F.J. Arnau, L.M. García-Cuevas, V.H. Farias

CMT Motores Térmicos, Universitat Politècnica de València, Spain

Abstract

Oxy-fuel combustion concept is studied in a compression ignition engine (CIE) using Mixed Ionic-electronic Conducting Membranes (MIECs) to separate oxygen (O_2) from air in order to achieve a clean combustion eliminating completely nitrogen oxides (NO_x) emissions and enabling upcoming carbon dioxide (CO_2) capture. Exhaust gas recirculation (EGR), composed mainly by CO_2 and water, is used to control the in-cylinder temperature and exhaust gases wasted energy is recovered for producing the O_2 required by the engine by heating up the MIEC. For this purpose, different engine configurations are analyzed in order to find out an optimum one in terms of energy efficiency and engine performance. Basically, two different EGR control systems (CS) are studied: one with a variable geometry turbine (VGT) on EGR line and other with a VGT on cylinder exhaust line. A simulation software, so-called Virtual Engine Model (VEMOD), is employed in this study to build and analyze the proposed oxy-fuel engine model which is calibrated with experimental data. The engine and its auxiliary components (turbochargers and heat exchangers) are assessed under oxy-fuel combustion conditions for the engine full load operation points from 1250 rpm to 3500 rpm. If compared to a conventional CIE, at high engine speeds the proposed oxy-fuel combustion engine provides similar brake power and indicated efficiency, whereas at low engine speeds, despite of it yields higher brake-specific fuel consumption (BSFC on average, more than 10%), a brake power enhancement (on average, more than 30%) is observed. In any way the breakthrough result is the feasible end of correlation between BSFC and CO_2 emissions due to CO_2 capture.

Keywords: Oxy-fuel combustion, Internal combustion engine, Membrane, MIEC, Energy recovery, Carbon capture

1. Introduction

Nowadays, as the effects of global climate change are clearer and the emission regulations are increasingly stricter, many of the main governments and economic agencies around the world are looking for new industrial projects based on sustainable development which help the productive sectors to turn their activities more environmentally friendly, whereas improving the efficiency of their processes as well. To illustrate that, the European Union has defined ambitious targets for 2030 such as at least 40% cuts in greenhouse gas (CO_2, CH_4, N_2O, Fluorinated gases, etc.) emission (GHG) and at least 32.5% improvement in energy efficiency [1]. The transport sector represents almost 25% of Europe's GHGs and the road transport is by far the biggest emitter responsible for more than 70% of all GHG emissions from that field [2]. Thus, effective solution, such as synthesis of e-fuels (synthetic fuel with low environmental impact), energy saving improvement of equipment [3] and development of systems with low or zero tank-to-wheel (TTW) emissions [4] [5], are claimed to improve

the existing internal combustion engines (ICEs) since they constitute almost 10% of worldwide emissions from fossil fuels [6].

Therefore, considering the concerns about climate change because of carbon dioxide (CO_2) emissions and local air quality deterioration due to transport requirements because of nitrogen oxides (NO_x), carbon monoxide (CO) and hydrocarbons (HC), the oxy-fuel combustion appears as one of the most promising solutions to eliminate those pollutants while maintaining energy conversion efficiency [7]. Abraham et al. were the first ones to propose the oxy-fuel combustion concept which was focused on enhanced oil recovery (EOR) removing the CO_2 purification required in flue gases recovery [8]. Currently, the oxy-fuel combustion technology is especially applied to thermal power generation industry focused on coal-fired power plant [9] [10] [11] [12] [13], biomass-fired power plants [14] and high-velocity oxy-fuel coating processes [15]. Moreover, its usage is assessed to be employed for refining sector [16] and cement production [17].

The oxy-fuel combustion concept may be defined as a combustion processes which takes place under highly oxygen-enriched conditions, using the exhaust gas recirculation (EGR) composed of CO_2 and water vapor to control the high combustion temperatures preventing overheating issues [18] [19]. That technology applied to ICEs is quite novel and there are few works available in the literature [20] [21] [22]. At the best of authors knowledge, this is the first work analyzing the feasibility of oxy-fuel combustion in a whole full load range of operation of a multi-cylinder CIE. Once the NO_x is produced due to high nitrogen concentration in air and high temperature inside combustion chamber in ICEs [23], if the fuel is burned with a gaseous mixture of O_2, CO_2 and H_2O instead of air, such as occurs in oxy-fuel combustion, the NO_x emissions are eliminated. Consequently, sophisticated-and-expensive NO_x after-treatment systems may be completely removed. Moreover, the combustion process may be optimized without the trade-off between NO_x and other pollutants emissions [20]. Therefore, the engine is fully optimized for lean burn (the fuel is burned with an excess of oxygen) [24] which may virtually eliminate the soot and CO emissions, and the combustion products are mainly CO_2 and H_2O.

Indeed, there have been several researches focus on oxy-fuel combustion in single cylinder engines, and the first proposal for that application in ICE was published by Osman et al in 2009 [20]. In their work, pure oxygen and water are directly injected into combustion chamber with diesel fuel and any intake valve is required. Once water has high specific heat capacity, it is used as a working medium for heat absorption, which also controls the high in-cylinder temperature, and for gas expansion during the expansion stroke. Thus, their results show a combustion efficiency enhancement which reduces the HC, CO and particulate matter (PM) emissions and surely minimizes NO_x formation as well.

An experimental campaign was carried out by Blarigan [21] to study the oxy-methane-fueled combustion in a spark-ignited engine. They analyzed the engine's performance under both wet and dry EGR conditions with various O_2 concentrations comparing them to methane-in-air operation. It was noted that the peak fuel-conversion efficiency for both wet and dry EGR under oxy-fuel combustion condition is lower than for methane-in-air operation, because the EGR working fluids have lower ratio of specific heats when compared air (with N_2). To improve the cycle efficiency based on oxy-fuel combustion in compression ignition (CI) engine , Zhe Kang et al [22] studied the effect of water injection through Computational Fluid Dynamics (CFD) simulations analyzing the injection timing, injection temperature and water amount. Therefore, the purpose is to couple the Otto cycle with the Rankine cycle [25] [26] [27] because steam may work as the main working fluid. They have found an optimal injection strategy with 1:1.11 fuel-to-water ratio, 365^{o}CA timing and 160^{o}C

temperature, enhancing the cycle efficiency by 5.2% compared to simulation without water injection.

Investigations have emerged motivated for simultaneously exploring the combined effects of oxy-fuel combustion and Homogenous Charge Compression Ignition (HCCI) strategies [28] [29] [30] [31], since the latter presents low chamber temperature and lean equivalence ratio which increase the thermodynamic efficiency and decrease harmful soot emissions [32]. Mobasheri et al [33] have used CFD models to evaluate the influence of that combination on combustion characteristics and engine operating conditions in a CI engine. In that research the intake gases are mainly O_2 and CO_2, so O_2 should be supplied from a commercial oxygen cylinder and CO_2 is captured by condensing and separating water vapor from the exhaust gases, thereby some part of CO_2 is mixed with pure O_2 and the rest of CO_2 is compressed and stored in a designed tank. Among the main results, it may be noted that increasing the CO_2 concentration rises the overall specific heat capacity of intake flow which decrease the in-cylinder temperature and pressure during combustion phase, reducing the engine power and the thermal efficiency; and at low engine loads worsens the Brake Specific Fuel Consumption (BSFC). Indeed, Abdulrahman Mohammed et all [34] found similar results investigating the oxy-fuel combustion in a single cylinder engine under HCCI application through an experimental setup. The conclusions of their study show that the net indicated engine efficiency with O_2 and recirculated CO_2 is only 15% because mainly that case is operated under lower in-cylinder temperature compared to air combustion and, due to higher back pressure to produce required EGR, the pumping losses are also greater.

One of the pivotal benefits of oxy-fuel combustion is the convenience of CO_2 capture and storage to use it as product into circular economy, converting the CO_2 into carbon-based economically viable fuels [35]. For instance, Oleksandr proposes the gradual rise of photocatalytic, CO_2 polymerization, biohybrid, and molecular machine technologies to enhance methods of electrocatalytic CO_2 transformation into chemical fuels [36]. In 2019, Sharma et all [37] proposed an on-board CO_2 capture and storage unit with ICE using a temperature swing adsorption integrated with a turbocharger system to compress and liquefy CO_2 (via Rankine cycle) using the heat of exhaust gases. By means of energy and exergy analyses of their study, they state that the proposed system may capture 90% of the emitted CO_2 from engine, without any energy penalty. However, the oxygen separation is one of the main obstacles for the implementation of oxy-fuel combustion in means-of-transport engine since it requires more complex and high-priced systems to supply a high-purity oxygen on board. In fact, the off-board oxygen acquisition may not be a profitable solution for the industry due to storage and transport costs, and especially for the transport sector, that would entail an increment of weight in vehicles leading to a fuel consumption deterioration.

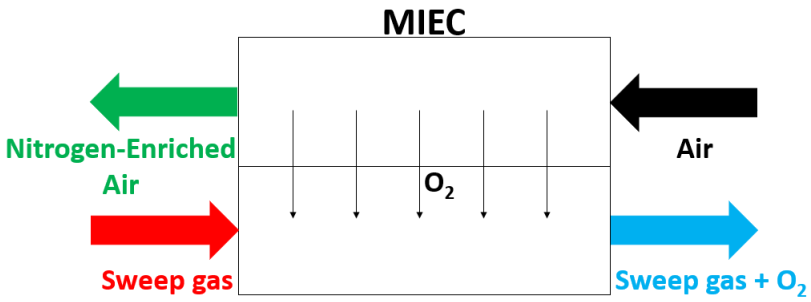

Figure 1: Macroscopic schematic representation of oxygen permeation through MIEC

Some solutions for oxygen separation have emerged such as cryogenic air separation (CAS) which may provide high-purity oxygen required on a large-scale application [38]. Nevertheless, that system involves a

relevant energy penalty and a high capital investment which complicates its proximity to market [39] [40]. In such a context, the oxygen transport membranes (OTM), also known as mixed ionic-electronic conducting membranes (MIECs), appear as an alternative to the previous technology, since they achieve economic saving of 10.5-17.5% and energy consumption reduction of 0.5-9% compared to CAS [40]. Despite there are some hurdles to MIEC's way towards industrial production due to some chemical and thermal stability issues under extreme environments [41] [42], growing breakthrough in performance of membranes indicates its potential application for in-situ and low-cost oxygen generation [43]. The MIEC transports oxygen from the feed side towards the permeate one by way of temperature and a partial pressure gradient between both sides, so oxygen molecules are adsorbed onto a porous, electrically conductive coating and dissociated into oxygen ions, which are transported through the non-porous electrolyte [44]. Once oxygen ions have reached the permeate side, they recombine to form oxygen molecules and desorb from the surface of the membrane. In addition, electrons are transported at the same time in the opposite direction to keep the electrical neutrality of the MIEC [45]. Moreover, sweep gas may be employed to heat up the MIEC and to reduce the partial pressure of the permeated O_2, which enhances the O_2 transport driving force (Fig. 1). Thus, MIECs seems to be a feasible solution, considering its simplicity and low cost, to produce oxygen from air for a clean combustion in CIE as described in this work.

Although the $Ba_{0.5}Sr_{0.5}Co_{0.8}Fe_{0.2}O_{3-\delta}$ (BSCF) membranes present some limited stability, that material has a high oxygen permeation with production capacity of up to $62\,mL\,min^{-1}\,cm^{-2}$ of oxygen at $1000\,^{\circ}C$ [46]. Thus, Serra et al. [47] conducted a characterization study of oxygen transport in BSCF MIEC based on an experimental and numerical assessment, analyzing some effects such as MIEC temperature, feeding flow, sweep inlet flow and sweep gas composition (oxygen dilution with CO_2, H_2O, He or Ar) on the MIEC performance. Their results show that increasing the temperature from $700\,^{\circ}C$ to $1000\,^{\circ}C$ improve the oxygen transport; the oxygen flux presents an asymptotic behavior regarding feed and sweep inlet flows; and the higher the molecular weight of the sweep gas is (such as CO_2 and H_2O), the better the oxygen is swept. Therefore, considering the oxy-fuel combustion technology to capture the CO_2, BSCF membranes arise as an oxygen separation way in ICE, using the exhaust gas as a sweep gas and taking advantage of its high thermal energy to generate enough pressure and temperature on MIEC feeding side to produce the needed oxygen for the proper engine performance under oxy-fuel combustion conditions.

Finally, the main objective of the current work is to highlight the high feasibility potential of the oxy-fuel combustion in CIE to eliminate NO_x, H_xC_y, CO and soot emissions, and to foster the capture CO_2. For this purpose, a CIE model is proposed and two EGR control system (CS) are studied with different heat-exchanger-and-turbocharger disposals to recover the exhaust gas energy which shall be used for the oxygen production and to make possible future CO_2 capture process. The ICE oxy-fuel combustion layouts studied are based on the preferred realizations patented by Desantes et al. [48]. Furthermore, a BSCF MIEC 0D-modela MIEC model based on results obtained by Serra et al. [47] is employed as a from-air oxygen provider and, thereby, the molar flux of oxygen may be expressed as function of the MIEC temperature and oxygen partial pressure gradient as shown in equations 1 and 2. Therefore, one may see that temperature has a key effect on oxygen production due mainly to its exponential dependence whereas the oxygen partial pressure ratio only has relevant impact when high MIEC temperatures (around $1000\,^{\circ}C$) are employed as presented by Serra's work. The authors have not found any published work in the literature studying the feasibility of oxy-fuel combustion in CIE with in-situ O_2 generation by means of MIEC, hence the novelty of this manuscript.

$$J_{O_2} = K(T) \cdot \ln \frac{p_{feed,O_2}}{p_{permeate,O_2}} \cdot \frac{T}{L} \tag{1}$$

Where the parameter $K(T)$ is given by:

$$K(T) = A \cdot \exp\left(- \frac{E_a}{T \cdot R} \right) \tag{2}$$

The manuscript is structured as follows: first, the model is described in section 2; then the results are presented and discussed in section 3; finally, section 4 includes the main conclusions of this work.

2. Model Establishment

All engine models used in this study are built and implemented in a non-commercial and in-house simulation software so-called Virtual Engine Model (VEMOD) [49] which has been developed by CMT – Motores Térmicos and previously used to evaluate energy fluxes in engines [50]. VEMOD presents specific sub-models for the 1D gas dynamics, boosting system, air-charge and EGR coolers, throttle valves, heat transfer including gas-to-wall heat exchange and wall temperature prediction, aftertreatment sub-models [51], etc. Also, VEMOD has been modified to add a BSCF MIEC 0D-model proposed by Serra et al. [47] which is composed by two sub-models (feed and permeate sides). The MIEC model calculates the oxygen transfer, which occurs isothermally, as a function of the feed temperature and oxygen partial pressure gradient between feed and permeate sides. For each side, a geometric mean of inlet and outlet compositions is used to determine the concentration of each component, and mass and energy balances are performed taking into account the heat transfer between both sides. Thus, all those mentioned sub-models are integrated into VEMOD to simulate the engine under steady-state and speed-and-load transient conditions.

2.1. Validation study (Baseline)

A 2.2 L turbocharged and direct injection compression ignition (CI) engine is used as a baseline for the oxy-fuel combustion model. Thus, a model of this baseline engine has been developed in VEMOD and calibrated using experimental data to reproduce a state-of-the-art Euro 6d full (E6d full) engine behavior. Once the model adjusted, an optimization procedure was carried out to analyze how far the engine performance could go if worked close to its thermal-mechanical restrictions with 2021 available state-of-the-art turbochargers. These results were thereby employed as optimized baseline engine to set limits and define objectives to be pursued with the oxy-fuel combustion engine. Fig. 2 shows the results of the calibration process for some of key parameters (torque and air mass flow) as well as the optimized (Opt) model points. One may see that that the calibration of the engine model is good. Authors consider that enough to guarantee a reliable extrapolation to the on-site O_2 generation concept studied for oxy-fuel combustion.

2.2. Implementation of the Oxy-fuel combustion concept

After having the model calibrated, the four cylinders as well as the intake and exhaust systems of the baseline engine are preserved, and original supporting devices such as heat exchangers (HEs) and variable geometry turbocharger (VGT) are removed and replaced by a new heat-exchangers-and-turbochargers layout in order to adapt the original engine to the oxy-fuel combustion. Thus, using one of the preferred realizations from authors' patent as baseline [48], the number of HEs and turbochargers as well as their sequence were tested

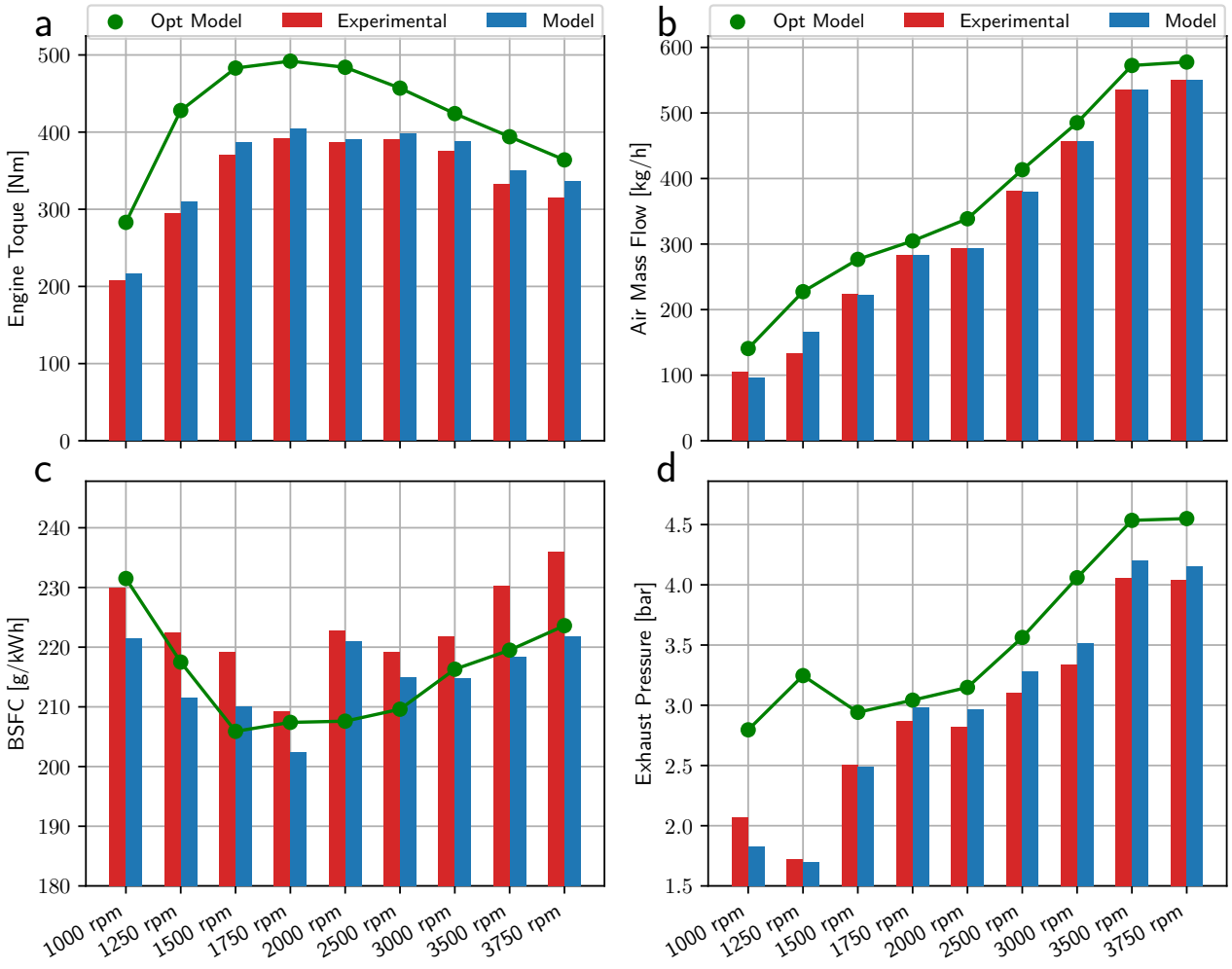

Figure 2: Comparison between Model and Optimized Model (Opt Model) results with experimental data for the base turbocharged IC standard air engine.

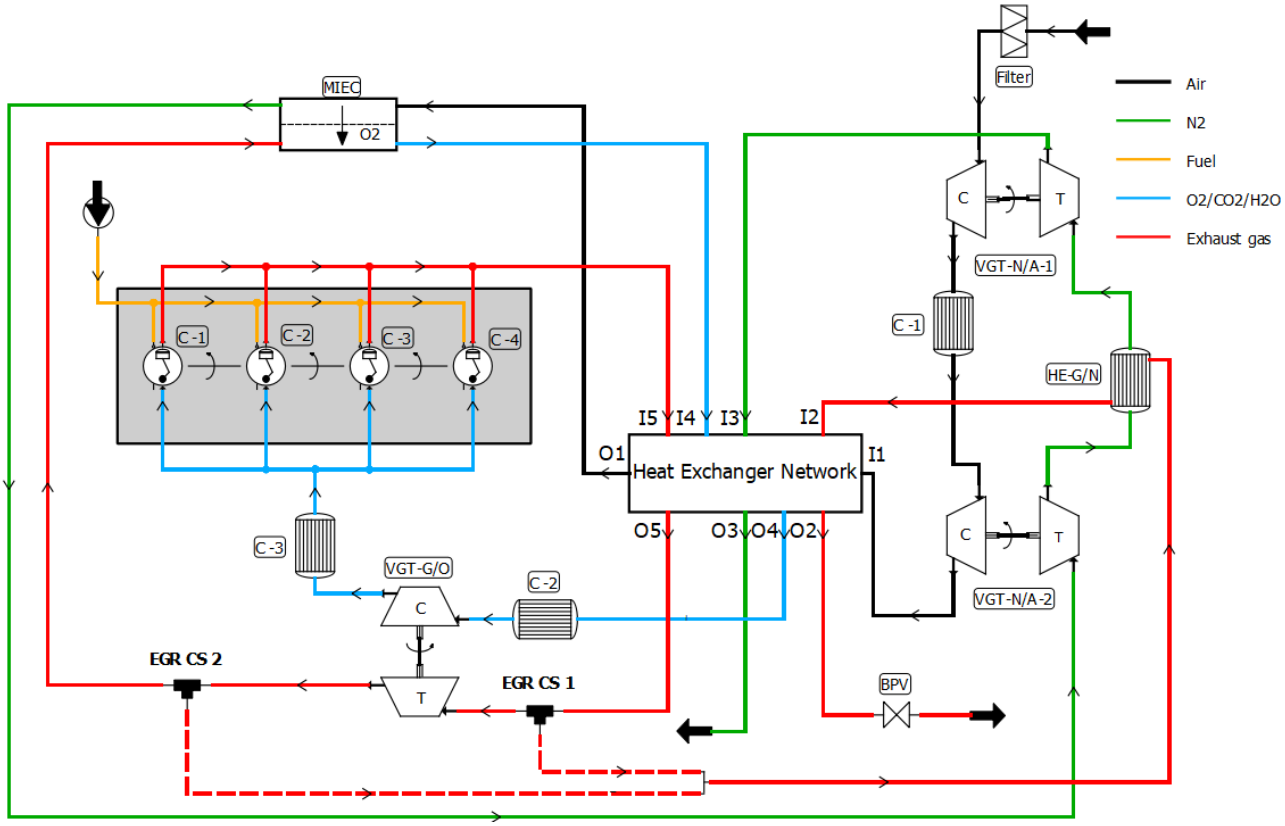

Figure 3: Implementation of the oxy-fuel combustion concept for two EGR control systems: CS 1 and CS 2

by putting them in series, in parallel and combining both configurations, controlling the flow split by means of actuators on the valves. Finally, after testing several heat-exchangers-and-turbochargers layouts, the one that presents the best results in terms of energy recovery, engine efficiency and packaging is analyzed in this study with two different EGR CSs (see Fig. 3).

The different fluids are described as follows:

- The orange line represents the fuel flow.
- The black line represents air flow.
- The green line represents a nitrogen-enriched flow.
- The red line represents the exhaust gas flow composed mainly by CO_2 and water.
- The blue line, also called oxidizer line, represents a blend composed by O_2, CO_2 and water which enters the cylinders.

For details about the layout conception one may read previous authors' patent [48]. For the purpose of this paper and in short, once the membrane requires high pressure and high temperature on its feeding side, a regenerative Brayton cycle with intermediate cooling and reheating between compression and expansion stages, respectively, is formed by the black and green lines. The regenerative Brayton cycle is linked to the CI cycle via the MIEC that replaces the combustion chamber in conventional Brayton cycles. The regeneration in the Brayton cycle uses energy from nitrogen-enriched line but also regeneration is used to cool down oxidizer line and CO_2 + H_2O line for easier further CO_2 capture. Thus, the regenerative Brayton cycle is mainly composed by two turbochargers put in series at the system entry to compress air up to about 5 bars, and by several HEs distributed in order to recover heat from exhaust gas and raising the temperature on the feeding side of the

MIEC up to about 900 °C.

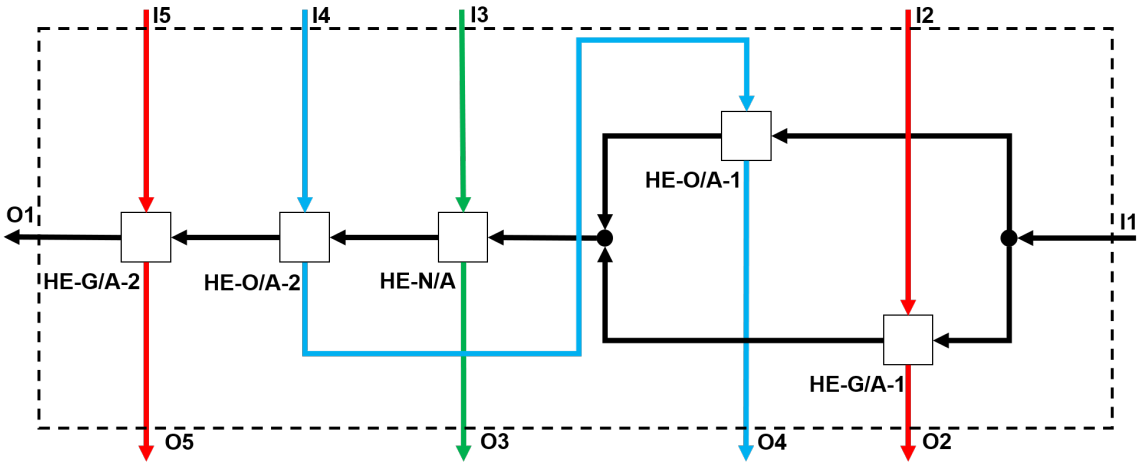

Figure 4: Heat exchanger network

Therefore, air enters the system, pass through two compression steps with intercooler and, before reaching the MIEC feeding side, is heated up firstly by an element called Heat Exchanger Network (HEN) (see Fig. 4). The Cooler C-1 role is to avoid damaging the VGT-NA-1 compressor reducing its inlet temperature and to increase compression efficiency. The HEN is composed by two HEs in parallel and three HEs in series: HE G/A-1 and HE G/A-2 recover energy from exhaust gas line; HE O/A-1 and HE O/A-2 cool down the oxidizer line while they raise air temperature; and HE-N/A tries to heat up air with residual thermal energy of the nitrogen line when HE G/A-1 and HE-O/A-1 may not supply enough energy. The nitrogen-enriched flow leaves the MIEC and is submitted to two expansion steps with intermediate reheating to convert the warmed-nitrogen energy into compression energy on the air compressors. For this purpose, the heat exchanger HE G/N retrieves the exhaust gases heat to enhance the VGT NA-1 performance increasing the inlet temperature of VGT N/A-1.

The oxygen permeated in the MIEC is diluted by the EGR which lowers the oxygen partial pressure at permeate side, improving oxygen production driving force and controlling exhaust gases temperature (red line) at cylinders outlet below acceptable limits. Furthermore, the EGR maintains the high combustion temperature under reasonable levels. Afterwards, the oxygen-enriched oxidizer gas (blue line) is cooled down, primarily by air (at HE O/A-2 and HE O/A-1) and thereafter by the cooler C-2 before reaching the VGT GO compressor, whereby it is pressurized. In addition, before entering the cylinders, the oxygen is cooled down again by the cooler C-3 for improving the volumetric efficiency of the intake gas raising its density.

For EGR control system 1 (EGR CS 1), depicted in Fig. 3, the combustion products leave the cylinders, rise the temperature upstream of the MIEC (at HE G/A-2), and are split off into two flows: the EGR and the exhaust gas which flows out of the system. The EGR flow is expanded into the VGT GO turbine, reducing the MIEC permeate side pressure. On the other hand, the exhaust gas leaving the system is twice cooled down, transferring its heat to regenerative Brayton cycle via HEN and HE G/N (see Fig. 3), and pass through a back-pressure valve (BPV) which, along with the rack position of the VGT GO turbine, controls the exhaust manifold temperature. The EGR control system 2 (EGR CS 2), depicted in Fig. 3, is similar to CS 1 and the main difference between them is the VGT GO turbine spot. Whereas CS 1 has the turbine on EGR line, CS 2 works with the turbine before the exhaust gas split and, thereby, their exhaust manifold temperature controls are different as it is further explained in subsection 2.3.

Attention should be drawn to the fact that the CO_2 capture is one of main purposes of this project so, even if the capture procedure itself is not described in this study, but it will be rather developed in future works. The presented layout tries to make easier this forward task, cooling down the CO_2, which leaves the system, as much as possible and expecting to capture CO_2 in super critical phase in upcoming researches.

2.3. Model description

2.3.1. General specifications

For each engine speed, the combustion behavior is governed and imposed by the heat release law obtained from the optimized model of the original engine with air combustion but removing the pilots injections for the sake of simplification, since there is still no available combustion law model properly adapted to oxy-fuel combustion application in available engine simulation software (neither in VEMOD nor in other standard commercial packages) being this also an objective for further works. In addition, the model is not able to predict the CO formation as well as soot emissions and, as a consequence, the hypothesis that the fuel is completely burned and oxidized is employed. This limitation is not relevant for the purpose of this work since, on the one hand, the literature shows examples of feasible and complete combustion in oxy-fuel combustion engines [20] [21] [22] [24] [32] [33] [34], and, on the other hand, the unique multi-cylinder engine analysis performed here at full loads (and with optimized heat release laws) is fully valid from the viewpoints of management of exhaust energy fluxes and gas dynamics, due to the low energy contained in CO and soot oxidation in CIEs. Nevertheless, for further part-load analysis of multi-cylinder engines a proper oxy-fuel combustion reduced order model is under development and will be object of future publications.

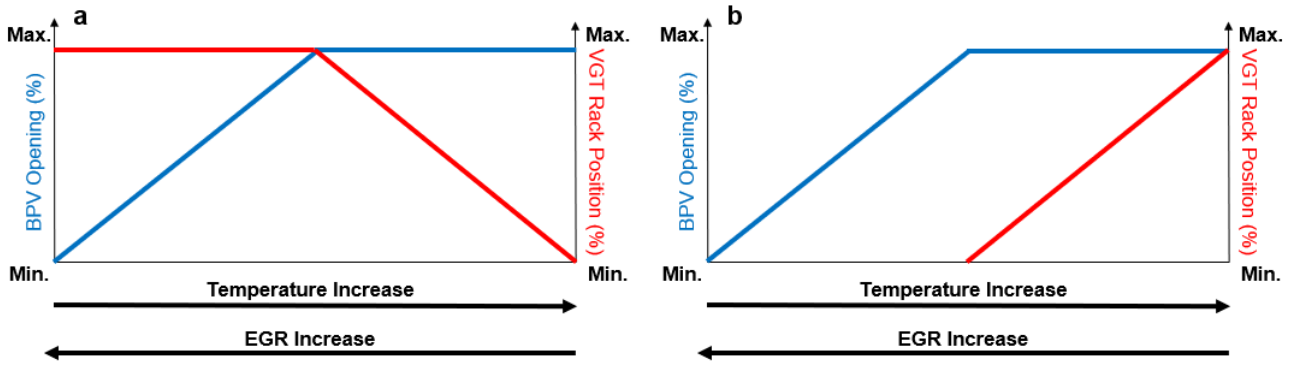

Figure 5: Exhaust manifold temperature control. (a) CS 1 ; (b) CS 2.

In this study the value of the oxygen–fuel equivalence ratio (λ) is kept constant and equal to 1.1; because on the one hand, since the combustion is carried out by compression ignition with an heterogeneous mixture, high λ improves the in-chamber flame diffusion and reduces soot formation; on the other hand, the oxygen production is costly because the MIEC requires high thermal energy to operate properly which precludes very high λ usage. In addition, this parameter is controlled by the injected fuel as a function of the amount of produced oxygen, which is a consequence of the boundary conditions imposed to the MIEC.

As mentioned above, high exhaust gas temperature is one of the key factors which impacts the suitable MIEC performance. In this way, after preliminary analyses of area and temperature needed for the proper functioning of the MIEC, which is further detailed in subsubsection 2.3.2, exhaust manifold temperature is fixed at 1000 °C and is controlled by two actuators in series: the BPV lift and VGT G/O turbine rack position. As seen in Fig. 5, which shows the temperature control strategy applied for CS 1 and CS 2, if the CIE requires higher

combustion temperature, the EGR rate must be reduced, increasing the cylinder inlet oxygen concentration and the combustion temperature as a result. For this purpose, the BPV is gradually open keeping the VGT rack at its maximum position for CS 1 and at its minimum position for CS 2, so at some moment, the BPV achieves the maximum opening and the rack position begins to be modified in a different way depending on CS in question. In CS 1, the rack is little by little closed diminishing the EGR rate because the turbine starts to be operated as a throttling valve under quasi-shock conditions. Whilst in CS 2, the rack is gradually open which decreases the turbine expansion ratio and, consequently, the compressor suction power, again reducing the EGR rate and CO_2 dilution.

The heat exchange and outlet temperatures of coolers and HEs are calculated based on a constant efficiency model (80% for coolers and 95% for HEs) and some simplifications are made such as the pressure drop on both sides of the HEs is negligible and the mass flow of coolant fluid used in the coolers (in this case water at room temperature) as well as its temperature are held constant. Those hypothesis are considered to calculate the transmitted power for defining specifications of HE facing a future component design. Since each turbocharger has a particular aim and specific flow conditions, their sizes must be different. Therefore, through similarity analysis [52], which may be automatically done by VEMOD defining a variable so-called "scale-factor", the turbocharger size may be either scaled up or scaled down with respect to reference one, in this case the baseline engine turbocharger is employed as reference. Thus, to find the best scale-factor for each turbocharger a multi-variable optimization process was carried out using the power of the engine operating at 3500 rpm as objective function to be maximized.

Since the air-nitrogen turbochargers are equivalent on both CSs and the VGT GO size found in one case may be used to estimate the scale of the same turbocharge in other CS, the optimization process was only performed for the CS 2. Thus, the scales obtained for VGT NA-1 and VGT NA-2 are 1.15 and 0.75 respectively, whilst the optimum VGT GO scale is 1.70. With regard to CS 1, the VGT GO scale was determined multiplying the EGR rate calculated in CS 2 (70%) by the optimum VGT GO scale found in that case, which results the value 1.20.

After studying the rack position impact of the nitrogen VGTs on engine performance, it has been noted that when those turbines operate at the turbocharger maximum efficiency point, with rack lift around 60%, the engine power is maximum for each engine speed. Thus, those air VGTs, which were initially specified in this project, could be replaced by fixed geometry turbochargers (FGT) operating with N_2, which are relatively simpler and more robust at high temperature operation.

2.3.2. Membrane area, Compression ratio (CR) and Start of Combustion (SOC) studies

.

A membrane area study was performed at 3500 rpm to find out the minimum area needed to supply enough oxygen for the proper engine operation. Fig. 6 shows on X axis the air temperature at the membrane entry and on Y axis the partial pressures ratio of O_2. This partial pressure ratio is defined as:

$$\Pi_{O_2} = \frac{p_{feed,O_2}}{p_{permeate,O_2}} = \frac{p_{feed} \cdot X_{feed,O_2}}{p_{permeate} \cdot X_{permeate,O_2}} \tag{3}$$

where p is the absolute pressure of the gas at each side of the membrane and X the oxygen molar fraction.

The level curves represent the membrane area necessary to produce the required oxygen at the full power point (3500 rpm). Using very large membrane areas would hamper the packaging of the final prototype, however,

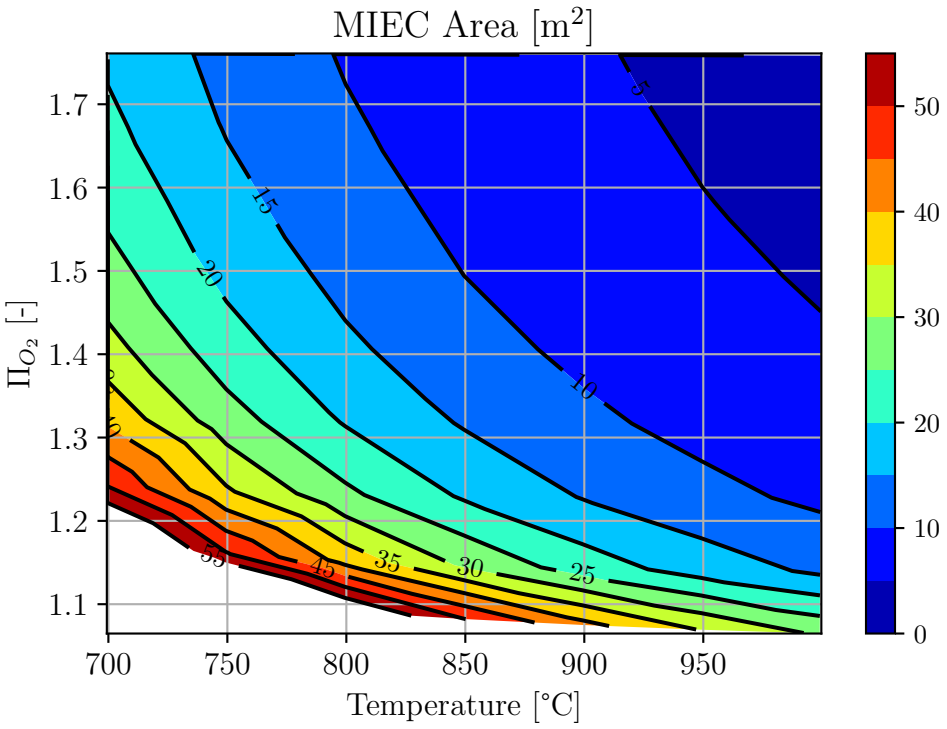

Figure 6: MIEC area needed to produce the maximum required O_2

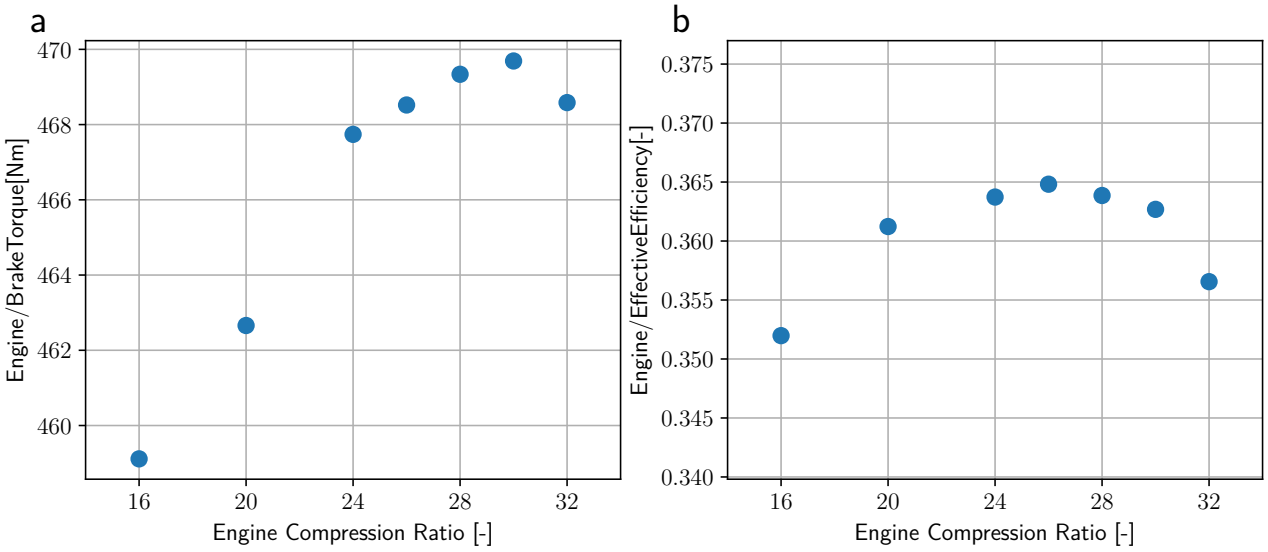

Figure 7: CR study at 2000 rpm full load. (a) Engine brake torque; (b) Engine effective efficiency

very small sizes may limit oxygen production or require pressures and temperatures which are inadmissible by the membrane mechanical structure. Therefore, taking into account above considerations, it has been possible to carry out the simulations with a $10\,m^2$ surface membrane, an affordable size when making a prototype, without loosing significant power and MIEC filtration efficiency, with a membrane inlet air temperature fixed at 1000 °C, the maximum temperature that the MIEC may withstand respecting its thermal-mechanical limits.

Since the baseline engine CR (original value = 16.2) had room for improvement due to lower trapped mass as a consequence of oxy-fuel combustion requirements (which means lower maximum in-cylinder pressure) and of engine efficiency, a sweep of CR was carried out taking into account the trade-off between the engine torque

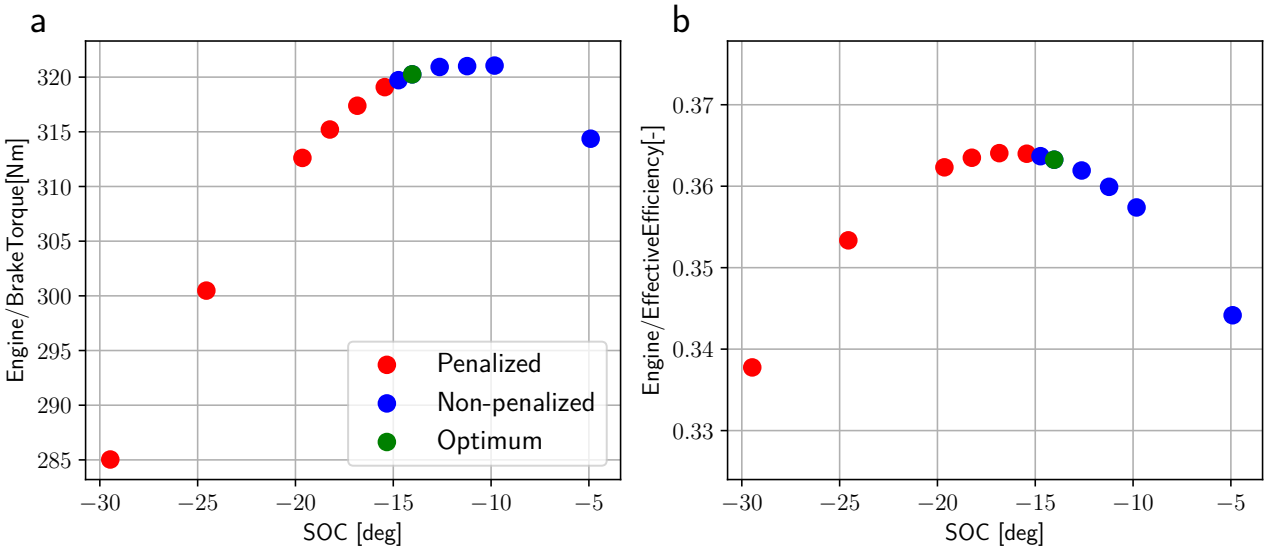

Figure 8: SOC-based sweeping study at full load for 3500 rpm

and effective efficiency at 2000 rpm (engine speed of minimum consumption for the optimized baseline engine), respecting the in-cylinder maximum pressure (180 bar) defined by the engine manufacturer. As shown in Fig. 7, within a CR range from 26 to 30, torque and efficiency are maximum without significant differences and, thereby, CR equal 28 is assumed as the optimum one.

Likewise, in order to find the best SOC and Start of Injection (SOI) for each engine speed and CS, a SOC-based sweeping process with constraints (Maximum In-cylinder Pressure $\leq$ 180 bar and Exhaust Manifold Temperature = 1000 °C) was carried out trying to maximize engine efficiency as well as torque as shown in Equation 4 and depicted in Fig. 8, whereby red and blue points represent SOCs with pressures higher (penalized) and lower than 180 bar respectively, and green point denotes the optimum SOC which maximizes the objective function in Equation 4.

$$\max_{SOC} \quad \text{ObjectiveFunction}(SOC) = \text{Efficiency}(SOC) \times \text{Torque}(SOC) \tag{4}$$

Finally, Table 1 summarizes the general model specification for each proposed CS.

3. Results and discussion

After having fixed key parameters like CR and membrane area at 3500 rpm (see Table 1) and determined the engine control procedure which is the same for each engine speed (using the BPV and VGT-G/O rack position to control the exhaust manifold temperature at 1000 °C, fuel amount to control λ, and maximizing the engine effective efficiency actuating on SOC), a full load engine speeds sweeping was carried out from 1250 rpm to 3500 rpm. In this section temperature, pressure and mass flows diagrams are analyzed for 3500 rpm (subsection 3.1), instantaneous results for lowest and highest engine speeds are compared (subsection 3.2) and average results from 1250 rpm to 3500 rpm are discussed (subsection 3.3).

Table 1: General specifications.

Parameter	CS 1	CS 2
VGT-NA-1 scale	1.15	
VGT-NA-2 scale	0.75	
VGT-GO scale	1.20	1.70
VGT-GO Min. Rack Position	5%	20%
VGT-GO Max. Rack Position	100%	
Min. BPV lift	1%	
Max. BPV lift	100%	
Exhaust manifold temperature	1000°C	
λ	1.10	
CR	28	
Membrane area	$10m^2$	

3.1. Temperature, pressure and mass flow diagrams

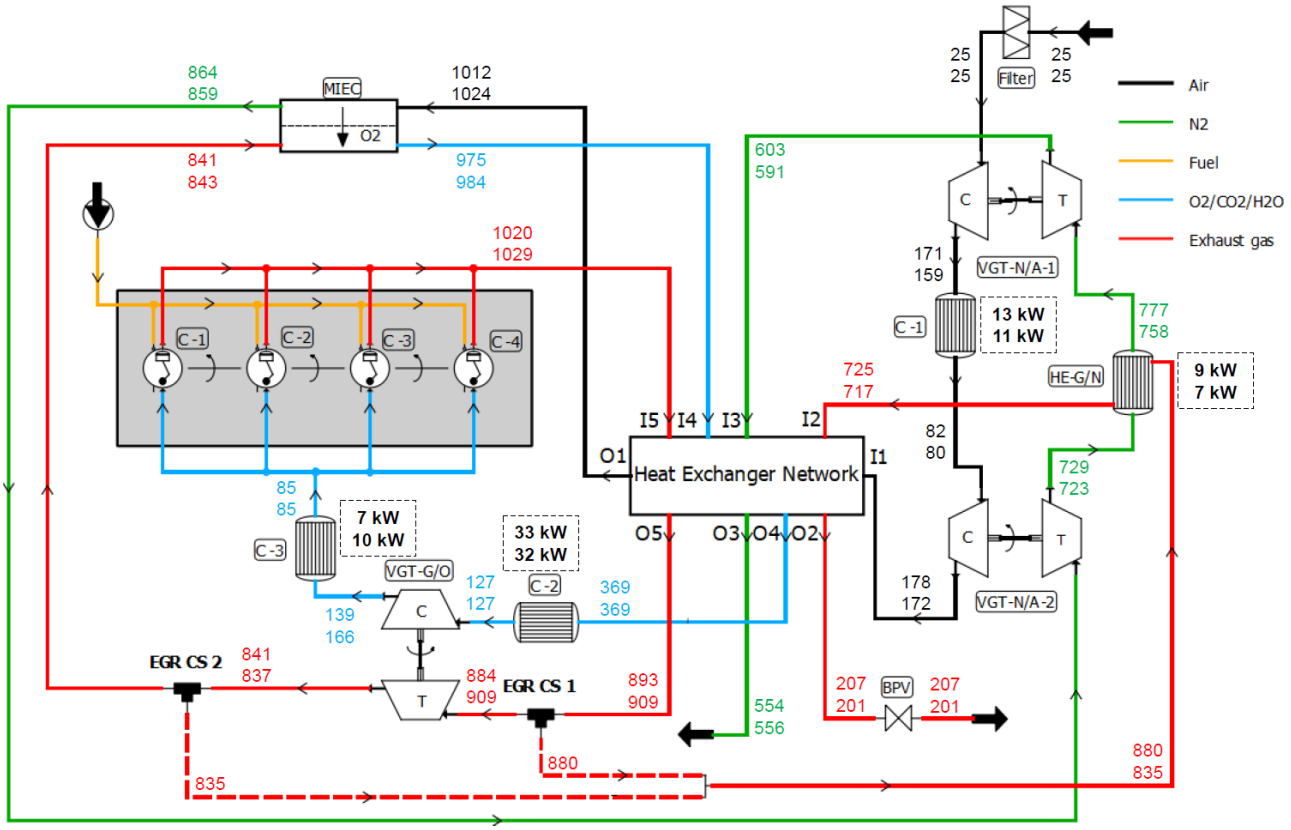

Figure 9: Power (in kW) and temperature (in °C) distribution diagram at 3500 rpm for EGR CS 1 (top values) and EGR CS 2 (bottom values)

Fig. 9 shows the power and temperature diagram for each EGR CS at the maximum rated power engine speed whereby the energy requirements are more important. Numerical values representing the calculated temperatures in degrees Celsius is added next to each flow line with top values for CS 1 and bottom ones for CS 2. In addition, the heat power exchanged is shown next to each HE and cooler following the aforementioned

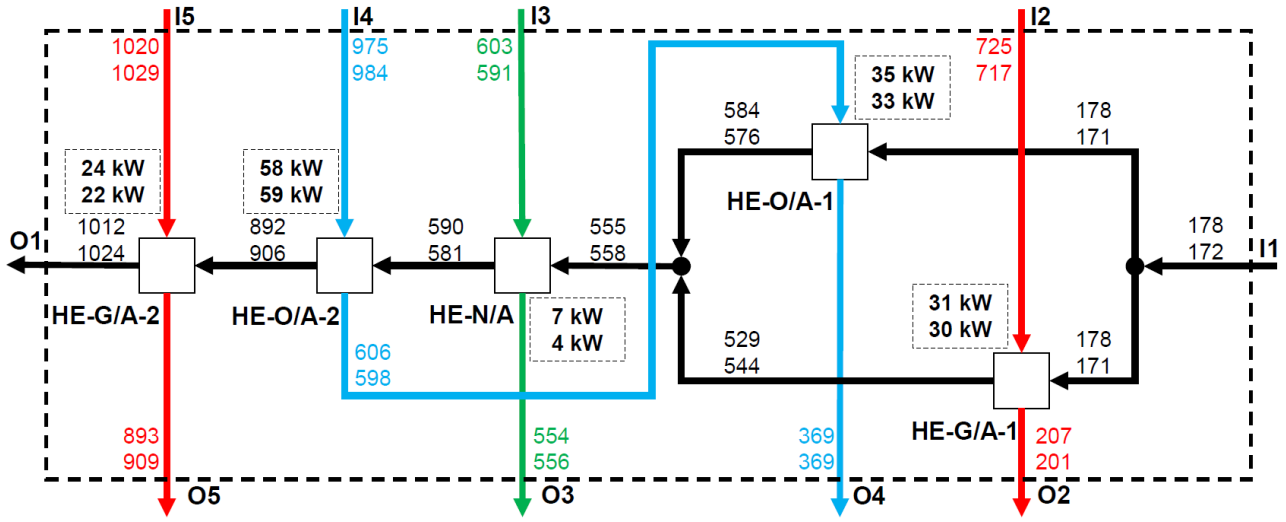

Figure 10: Power (in kW) and temperature (in °C) distribution diagram at 3500 rpm inside HEN for EGR CS 1 (top values) and EGR CS 2 (bottom values)

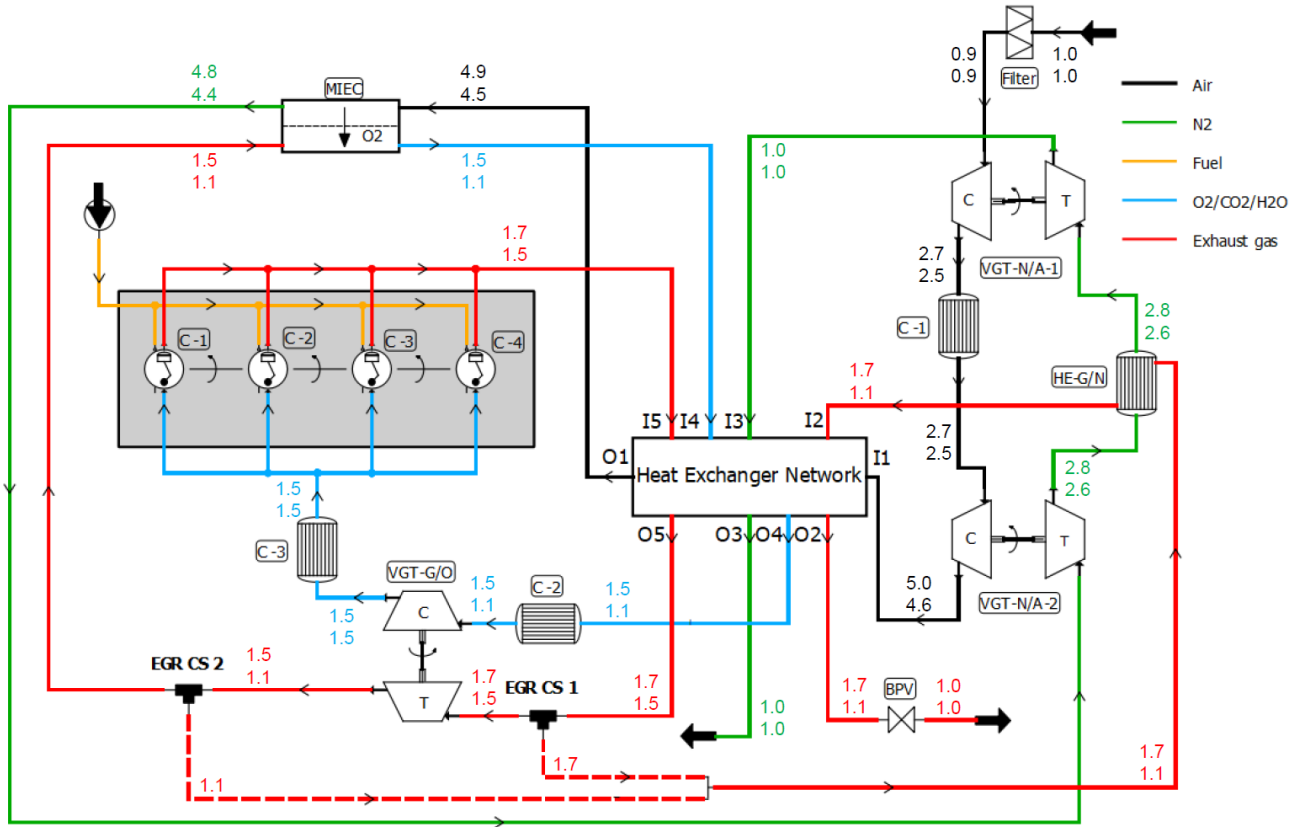

Figure 11: Pressure (in bar) distribution diagram at 3500 rpm for EGR CS 1 (top values) and EGR CS 2 (bottom values)

sequence. Also, the same power and temperature distribution is shown inside HEN (see Fig. 10). In general, as depicted on those diagrams, the two proposed CSs exhibit analogous results in terms of thermal energy distribution (a temperature difference of around 5 °C) and, in both cases, the HE-O/A-2 is the biggest HE (with approximately 60 kW power), so it may be separated into two or more HE (in series or parallel) in forthcoming acquisition. Although the HE-G/A-2 is the most crucial HE, since its outlet and inlet temperatures are very

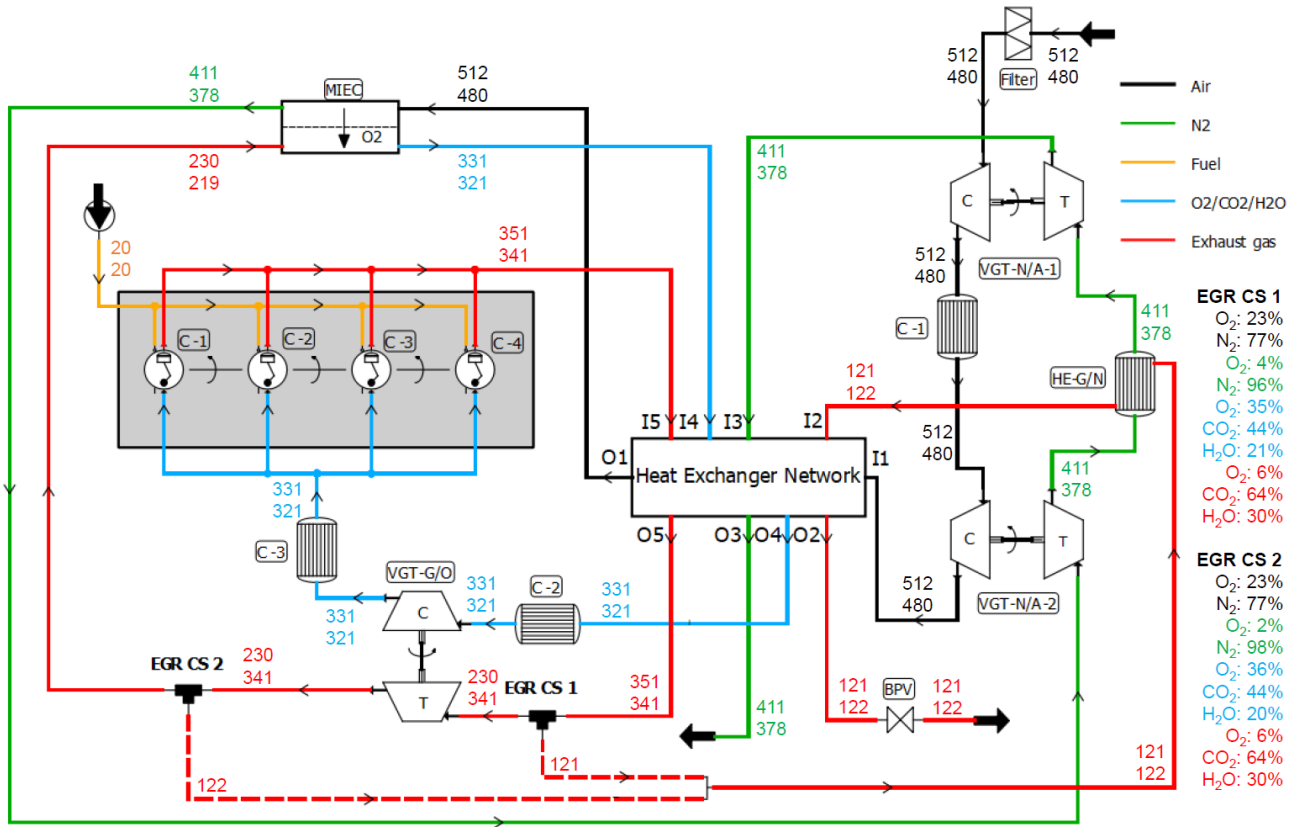

Figure 12: Mass flow (in $\mathrm{kg\,h^{-1}}$) distribution diagram at 3500 rpm for EGR CS 1 (top values) and EGR CS 2 (bottom values)

high (1000 °C) that may be a technological limitation, the other HE possess temperatures within orders of magnitude of those found in the road transport sector.

Fig. 11 and Fig. 12 show the effect of each EGR CS on pressure distribution and mass flow distribution respectively following the same representation scheme as for temperature diagram (with top values for CS 1 and bottom ones for CS 2). Although EGR CS 1 presents higher pressure than EGR CS 2 in Brayton cycle, as the EGR CS 2 may slightly yield higher temperature at MIEC feed side inlet and it posses lower MIEC permeate side pressure due to its VGT-G/O turbine expansion and BPV full opening which improve the MIEC filtration efficiency (comparing the mass fraction of oxygen at nitrogen-enriched line: 4% for CS 1 and 2% for CS 2), they produce similar amount of oxygen (around $101\,\mathrm{kg\,h^{-1}}$). For both CSs, all engine speeds analyzed in this work present similar exhaust gas composition with mass fraction of O_2 equal to 6%. Moreover, as depicted on Fig. 12, there is a mild difference (around $10\,\mathrm{kg\,h^{-1}}$) between CSs in terms of mass flow at brayton and CI cycles lines.

3.2. Instantaneous results

Fig. 13 shows the main in-cylinder instantaneous results for the lowest and highest engine speeds. The two proposed CSs possess analogous outcomes that distinguish from optimized baseline results especially in terms of in-cylinder oxygen content (Fig. 13d): the oxy-fuel combustion presents 15% more oxygen mass fraction than a conventional combustion, even though the trapped O_2 mass is lower in oxy-fuel combustion at 3500 rpm, since there is not enough thermal power in the exhaust gases to produce more O_2 in the MIEC at 1000 °C of exhaust gas temperature. Although the in-chamber temperatures are greater in oxy-fuel combustion due to its lesser inert concentration, they are not outrageous if compared to optimized baseline case (Fig. 13b).

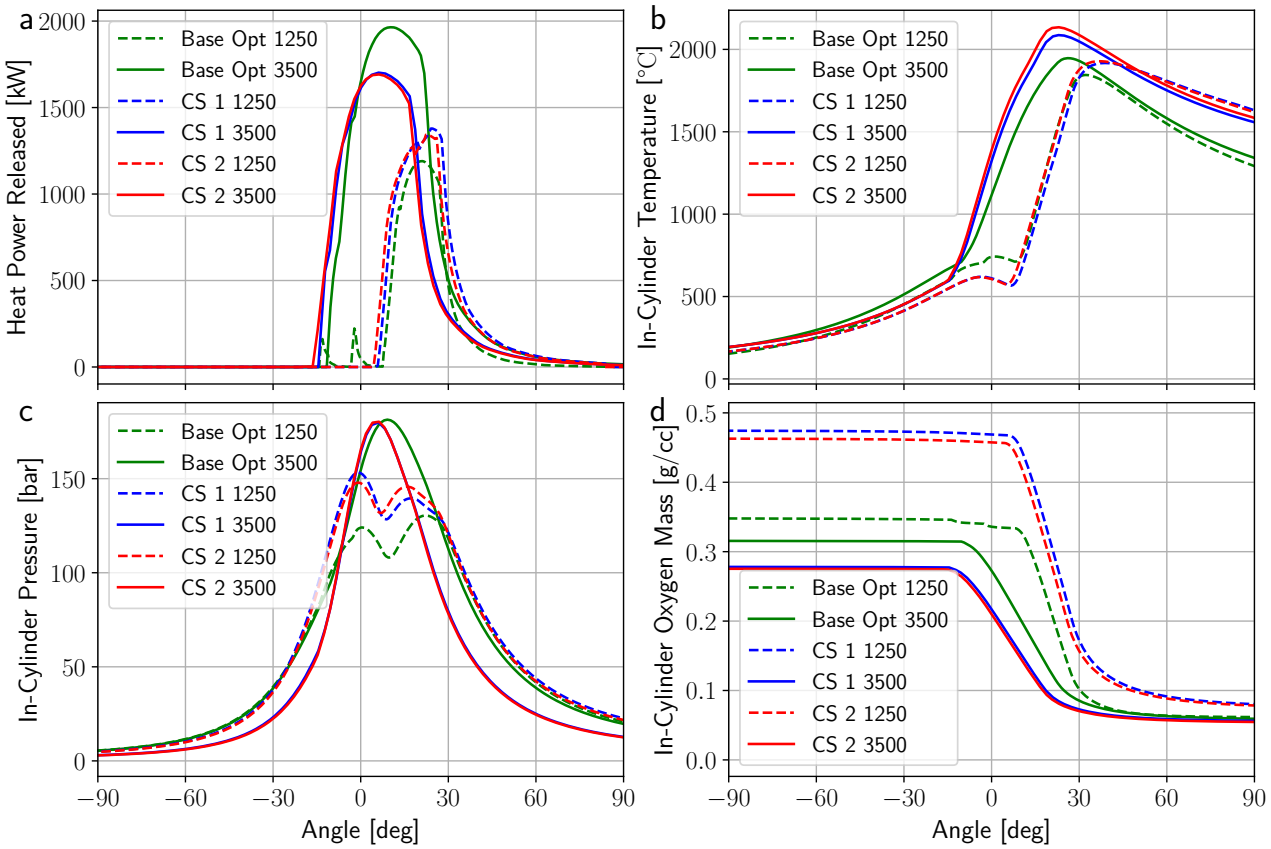

Figure 13: The instantaneous results of in-cylinder parameters at 1250 rpm and 3500 rpm full load

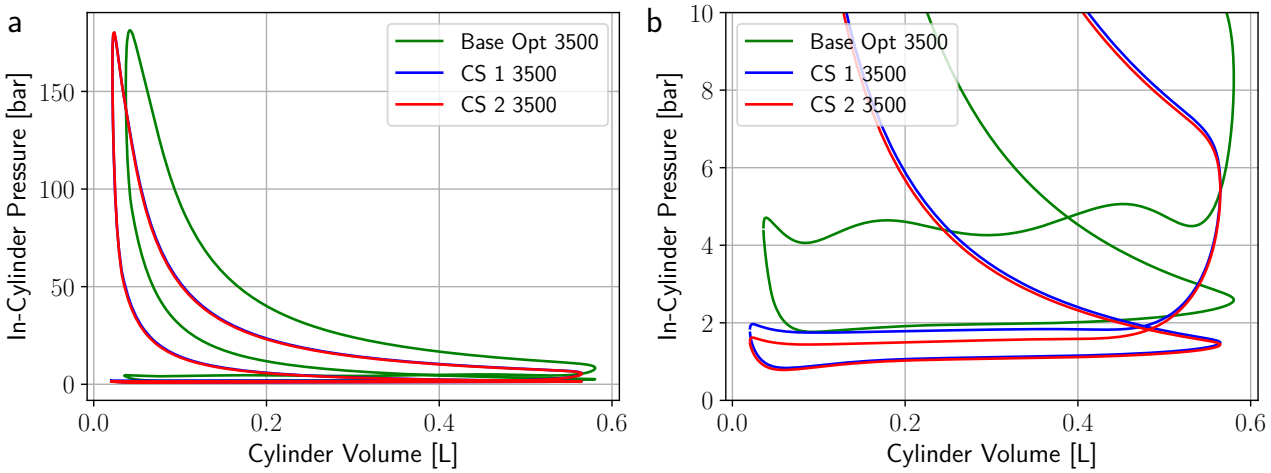

Figure 14: In-cylinder pressure-volume diagram at 3500 rpm full load. (a) Full diagram; (b) Zoom in on pumping loop

Fig. 14b shows the indicator diagrams for the highest engine speed. The effect of the compression ratio is observed in the minimum volume value of each cycle. The smaller amount of trapped mass combined with the characteristics of that trapped gas (with lower γ under oxy-fuel combustion conditions) lead to a smaller area enclosed by the high-pressure loop. However, part of this loss may be compensated by reducing pumping losses thanks to an air management system completely different from the conventional one.

As already mentioned, the SOC value has been optimized in terms of torque and efficiency by limiting the

maximum pressure inside the cylinder to 180 bar. At high speed, despite the increase in compression ratio in oxy-fuel combustion configurations, the lower in-cylinder pressure at IVC (Intake Valve Close) (Fig. 14b) causes pressure and temperature reduction during the compression stage (compare Fig. 13b and Fig. 13c), this allows a slight advance of start of combustion compared to the conventional engine without exceeding the maximum pressure limitation (Fig. 13c). It is observed how the trapped oxygen is a little less than in the conventional case (Fig. 13d) with the consequent reduction of heat released power (Fig. 13a). In addition, with the exhaust manifold temperature control, the oxy-fuel combustion cases present similar oxygen mass if compared to the conventional one, but with lower pressure at IVC (Fig. 14b), which may indicate that less diluents are trapped (in next subsection that behavior is detailed) due to lesser CR and lower cylinders intake pressure (Fig. 14b), which allows reaching a higher temperature at the end of the expansion (Fig. 13b).

Finally, at low engine speeds, the supercharging effect on the conventional CIE is much lower and, thereby, at IVC the pressure and temperature conditions are similar. Such an effect, combined with the higher CR and the possibility of achieving high oxygen concentrations in oxy-fuel combustion conditions, allows higher pressure values at the end of the compression stage but without exceeding the in-chamber pressure threshold (180 bar) (Fig. 13c). In addition, under these conditions the mass flows inside CI cycle are lower which decreases the membrane thermal requirements to produce the necessary oxygen. As can be seen in Fig. 13d the trapped oxygen is much higher than the conventional case. However, the need to have energy in the membrane forces the system not to prioritize the CI cycle performance optimization, delaying combustion and not reaching the maximum pressure limit value. For this preliminary study, pilot combustion was not used in oxy-fuel combustion cases as it can be observed in the case of conventional combustion (Fig. 13a). A more in-depth study of combustion will need to be carried out in future works.

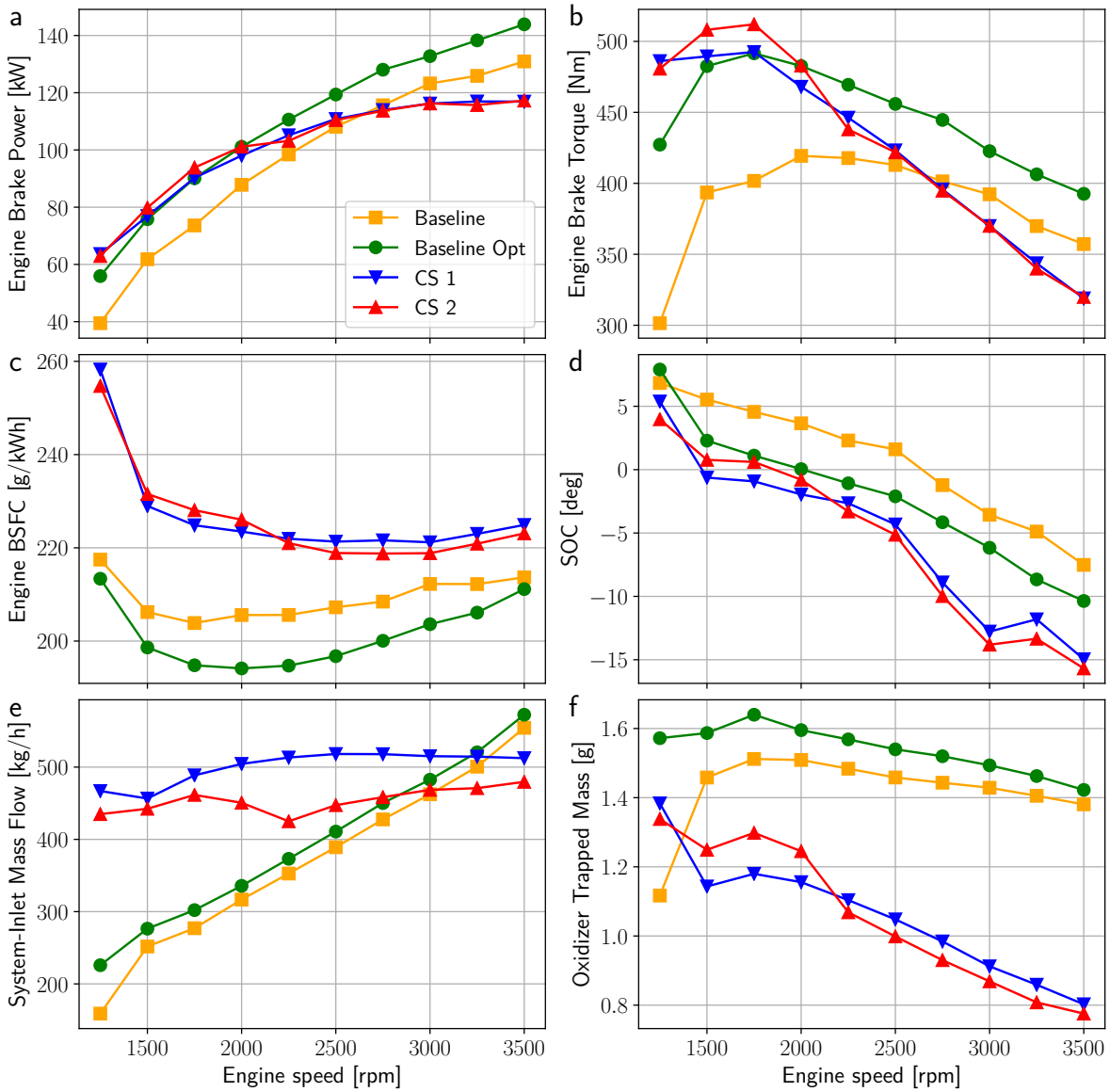

Figure 15: The average results of relevant average engine variables of oxy-fuel combustion EGR options (CS1 and CS2) compared to baseline and baseline optimized cases with air combustion engine (Baseline and Baseline Opt)

Although the oxy-fuel combustion presents lower torque than the optimized original engine at high engine speeds (Fig. 15a and b), if compared to original non-empowered engine, it provides similar brake power in such a zone and greater torque at low engine speed because the nitrogen turbochargers, working at their maximum efficiency points, seek to supply the maximum air flow regardless of engine speed (Fig. 15e). As the oxy-fuel combustion cases possess lower CR and cylinders intake pressure than the conventional one (Fig. 16e), less oxidizer mass is trapped (Fig. 15f). With respect to BSFC, even though the oxy-fuel combustion configurations present lower pumping losses than the air-based combustion ones (Fig. 16b), it may be seen that only at high engine speeds the oxy-fuel engines may achieve values similar to those offered by the conventional combustion engine with differences of around 30 g/kWh and 5 g/kWh at low and high engine speeds respectively (Fig. 15c). That is due to the fact that there is less thermal power available in the exhaust gases at low engine speeds

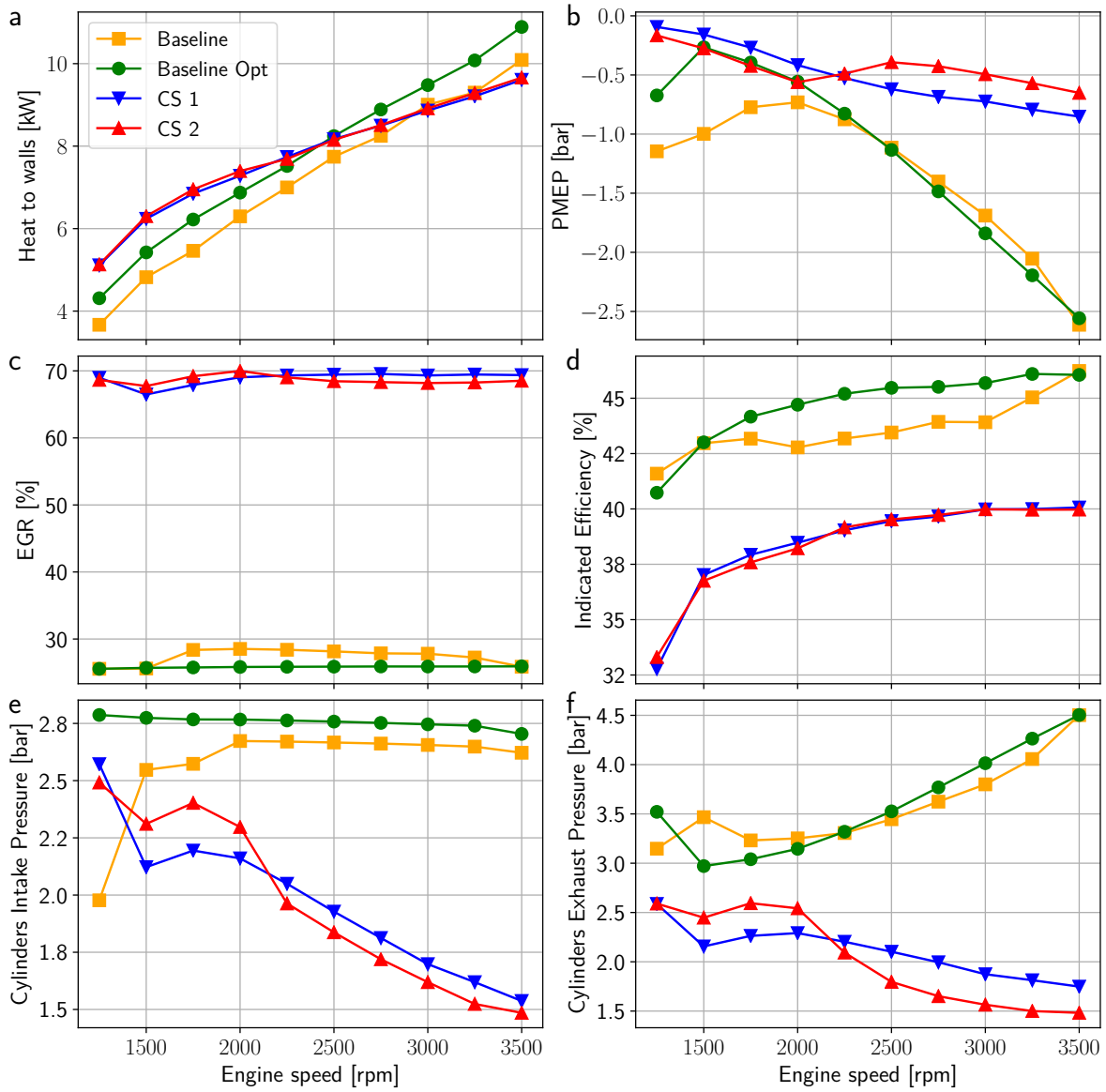

Figure 16: The average results of relevant average engine variables of oxy-fuel combustion options (CS1 and CS2) compared to baseline and baseline optimized cases with air combustion engine (Baseline and Baseline Opt)

to generate enough oxygen and the engine has to work under more delayed ignition conditions (Fig. 15d) in order to convert more heat power released at combustion process into thermal energy for the exhaust gases than into mechanical power. Furthermore, as the heat capacity ratio (γ) of the CO_2 and water mixture is lower than the γ of the N_2 [53], the engine indicated efficiency is lower for oxy-fuel combustion than for a conventional combustion. In addition, the oxy-fuel combustion temperature is higher which renders more heat losses (Fig. 16a) at low engine speeds. Despite such higher consumption, it must be taken into account that the oxy-fuel combustion engine is mainly designed to capture CO_2. Therefore, that purpose could compensate that energy consumption penalty, since BSFC is not correlated anymore with CO_2 emissions, and valorization of high-purity captured CO_2 could be used to partially compensate the increment in cost to owner due to higher BSFC.

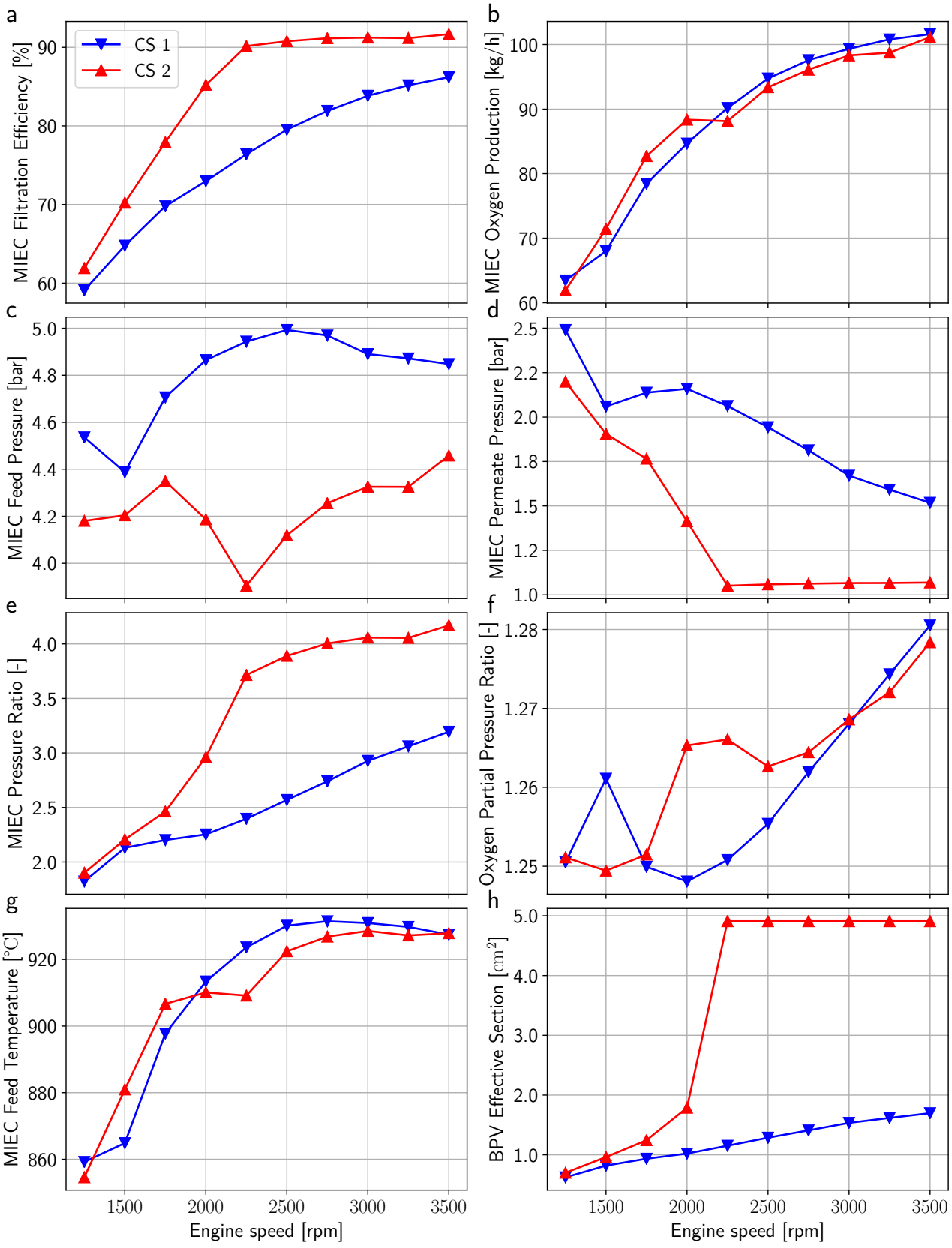

Figure 17: The average results comparing both EGR control systems: CS 1 and CS 2

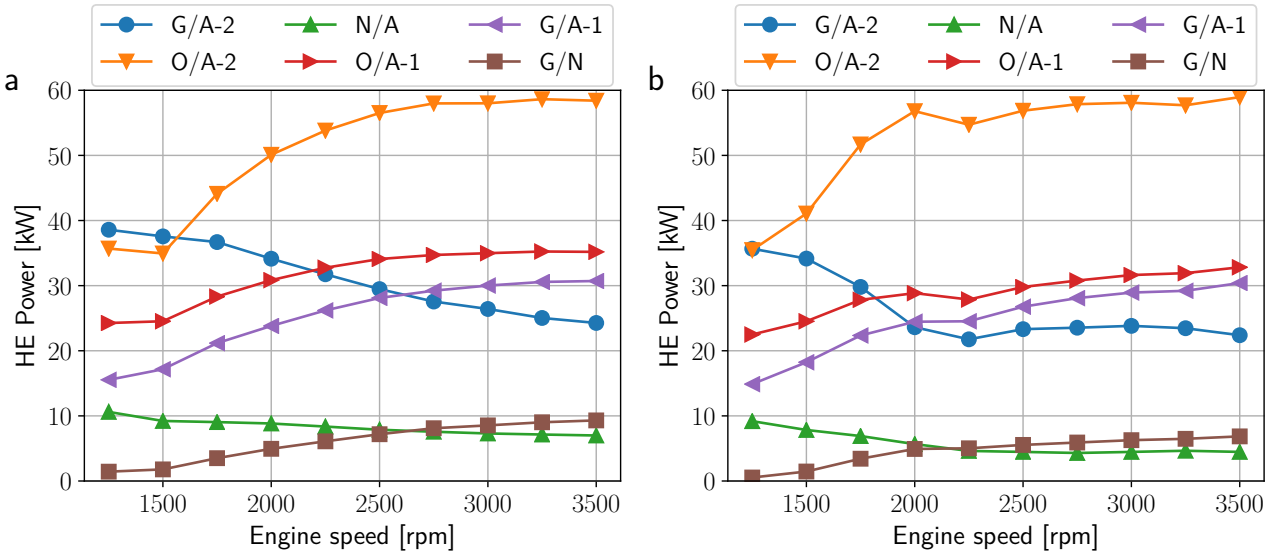

Figure 18: HE power average results: (a) CS 1; (b) CS 2

For CS 2, the MIEC filtration efficiency, defined by the ratio between the O_2 permeated in the MIEC and the total O_2 which enters the MIEC feed side, is almost constant at 90% when the back pressure valve is fully open (Fig. 17a and f), since the permeate pressure (also called back pressure) is low which entails a greater pressure gradient (Fig. 17a, c, d and e). Nevertheless, whenever the back pressure valve is slightly closed, the permeate pressure increases, reducing the partial pressure of O_2 gradient which impairs the MIEC filtration even if high temperatures are observed at the end of the expansion stage (Fig. 13b). Also, the mass flow of O_2 transferred in the MIEC varies in a similar way to engine power (Fig. 15a and Fig. 17b) with respect to engine speed, showing that the engine power only depends on total oxygen produced by MIEC (compare Fig. 15a with Fig. 17b).

In general, it has been noted that, for all engine speeds in both CSs, the EGR remains relatively constant at 70% to regulate the exhaust temperature. However, as mentioned above, the oxygen production decreases at low engine speeds leading to less mass flow at MIEC permeate side, so the Brayton cycle air exchange less thermal power with the CI cycle hot gases (oxidizer and exhaust gas in Fig. 4). Therefore, when that happens, the nitrogen line (green line in Fig. 3) energy becomes more useful to heat up the Brayton cycle air when the thermal powers provided by oxidizer and exhaust gases are insufficient, justifying by this way the HE N/A location (Fig. 4 and Fig. 18).

The compressors integrated in the Brayton cycle have the full load operating points gathered in small area of the maps (Fig. 19e, f, g and h) which makes easier their future selection and purchase. Furthermore, those compressors operate close to their maximum efficiency points with high compression ratios (from 2 to 3). Fig. 19c and d show the VGT GO maps of the CS 2 and two operating zones may be observed: the high engine speeds zone whereby the EGR is controlled by the VGT GO position; and the low engine speeds zone whereby the VGT position is fixed at its minimum position and the back pressure valve regulates the exhaust manifold temperature.

Regarding the VGT G/O of CS 1 (see Fig. 19a and b), it has been found that at full load points the exhaust temperature is only controlled by the back pressure valve working with the turbine completely open, which would be similar to not utilize any turbocharger in CS 1. However, this turbocharger has been kept in the

model in case its usage is required at other operating points (e.i. lowering the engine load).

In summary, the behavior differences between both layout can be enumerated as follow:

- At low engine speeds, EGR CS2 operates with higher cylinder intake and exhaust pressure (Fig. 16e-f) due to the energy recovered by the turbine (Fig. 19c-d). The pumping losses are higher (Fig. 17g) due to turbine back-pressure; the membrane efficiency is bigger (Fig. 17a) and so it is the O2 production (Fig. 17b).

- This allows to trap more mass at low engine speeds and more O2 (Fig. 15f), burn more fuel (working at constant equivalence ratio) and, thus, produce more torque (Fig. 15b). It also allows to introduce more EGR inside the cylinder (Fig. 16c). Due to this last effect, the oxygen mass fraction trapped inside the cylinder is then lower (fig13d), so the combustion needs to be slightly delayed (Fig. 15d) to obtain the desired exhaust temperature. This produces a loss in efficiency and an increase in fuel consumption (Fig. 15c).

- However, as the engine speed increases with EGR CS2 configuration, the backpressure valve must be opened to regulate the temperature (Fig. 17h) until it saturates at its maximum opening. After the maximum backpressure valve opening, the temperature is regulated varying the geometry of the turbine (VGT) (Fig. 5b). As the turbine opens, its capacity to recover energy decreases. Then, EGR CS2 is working with lower pressures in the permeate side of the membrane (Fig. 17d), what makes the feed side to also work with lower pressures if the partial pressure difference is to be kept constant. This reduces the mass flow passing through the Brayton cycle (Fig. 19f and Fig. 15e). With a lower mass flow in the feed side, the oxygen production is reduced even with a higher membrane efficiency, which presents an asymptotic behavior against the rotational speed (Fig. 17a).

- From all these results, on the one hand, can be concluded that EGR CS1 presents a smoother behavior throughout the whole full load curve, although with a lower low-end torque. The turbine placed in the EGR line (VGT-GO) does not work in any point of the whole full load line (fig19a-b), so it may be removed from this configuration leading to a decrease in the cost and complexity of the system.

- On the other hand, a configuration like EGR CS2 may have higher acquisition costs, but its low-end torque is higher, and its high-speed full-load power is like that of EGR CS1 with a reduced brake specific fuel consumption.

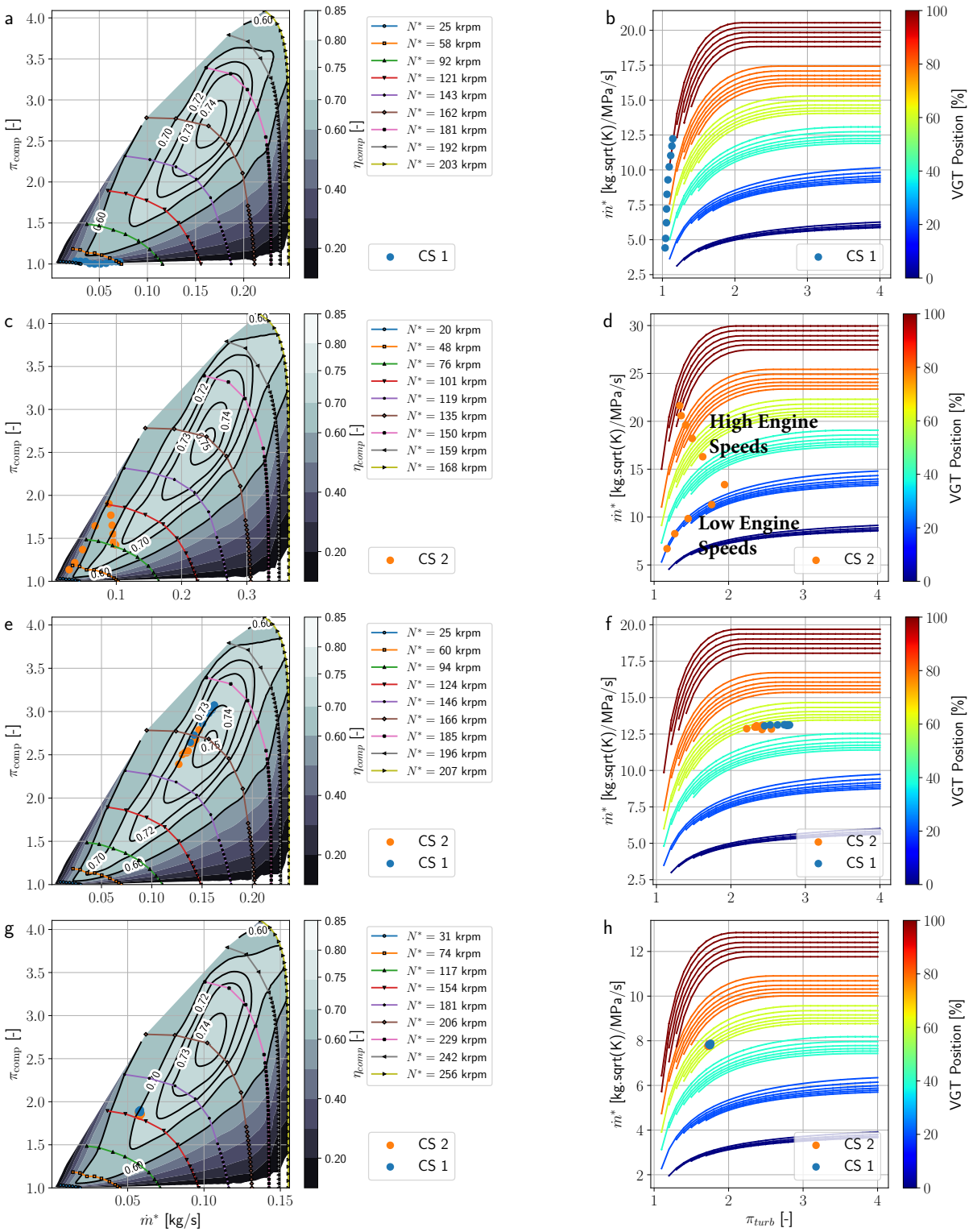

Figure 19: Turbochargers maps: CS1 VGT-GO (Compressor a and Turbine b), CS2 VGT-GO (Compressor c and Turbine d), VGT-NA-1 (Compressor e and Turbine f), VGT-NA-2 (Compressor g and Turbine h). The turbochargers maps presented in this work follow the nomenclature, terminology and representation standards applied to turbochargers recommended by SAE J1826 Reaffirmed MAR95 [54]

4. Conclusions

Through two different EGR control systems (CS 1 and CS 2) the oxy-fuel combustion concept is study in a compression ignition engine applying mixed ionic-electronic conducting membrane as a from-air oxygen provider. Thus, the two oxy-fuel combustion engine configurations are compared with each other and with conventional baseline and optimized baseline engine configurations for full load operating points from 1250 rpm to 3500 rpm.

The temperature, pressure and mass flow diagrams at 3500 rpm show that the two proposed CSs present similar results in terms of thermal energy and mass flow distributions because oxygen production mainly depends on regenerative Brayton cycle structure (HEs and turbochargers disposal) which is preserved in both CSs. As the global optimization objectives are the same with both configurations (same merit function, same exhaust gases temperature, same maximum efficiency objective in turbomachinery, ...) the global system converges to the same thermodynamic and flow variables with both CS1 and CS2. Moreover, in both cases the critical data, MIEC feed temperature and oxygen partial pressure ratio, which control the oxygen production for the engine proper operation varies similarly with respect to engine speed; i.e: from 860^{o}C to 930^{o}C and from 1.25 to 1.28, respectively. But the difference is how VGT-GO operates and, also, the size of this specific turbocharger. It is much bigger in the case CS2 than in CS1. Therefore, one conclusion is that CS1 is a more convenient solution in sake of layout simplicity and lower-cost, since on the one hand the turbocharger is smaller (lower inertia and lower cost). And on the other hand, it may be probably avoided when the whole engine is completed with the carbon capture subsystem, i.e.: VGT-GO in CS1 case is not more useful that a regulation flow valve or any other flow regulation system, since the compressor of CS1 does not provide any pressure

Comparing the instantaneous results, the oxy-fuel combustion cases distinguish from optimized baseline case especially with respect to in-cylinder oxygen content which, coupled with higher compression ratio, SOC optimization process and different control system in oxy-fuel combustion configurations, leads to higher in-chamber temperature and higher maximum pressure at 1250 rpm. Moreover, in spite of the oxy-fuel combustion presents a smaller area enclosed by the high-pressure loop due to its smaller amount of trapped mass and lower γ of the oxidizer, the pumping losses reduction thanks to a different engine control system may compensate part of that mechanical work loss.

The average results show that, if compared to a conventional CIE, at high engine speeds the proposed oxy-fuel combustion engine provides similar brake power and indicated efficiency, whereas at low engine speeds, despite of it yields higher brake-specific fuel consumption (BSFC on average, more than 10%), a brake power enhancement (on average, more than 30%) is observed. Also, there are not clear differences between the EGR CSs on engine performance, since they produce similar amount of oxygen as a result of both having same exhaust gas temperature and equivalent oxygen partial pressure ratio. In addition, one may see how the engine power with regard to engine speed is practically function of the oxygen production which is conditioned to membrane temperature and pressure ratio (between feed and permeate sides). Although VGT G/O of CS 1 seems to be useless at full load operating points, it may be required to control the engine in upcoming studies considering the CO_2 capture system and engine partial load points requirements.

Finally, although the EGR control systems present similar results in terms of engine performance, the EGR CS 1 proposal seems to offer more advantages regarding the engine exhaust gas temperature control in future operating points (at partial load conditions). Thus, the VGT G/O turbine of CS 1 may be useful at engine lower

loads, since the VGT rack would choke the EGR line when high temperature is required by the MIEC, whereas a valve would be necessary at that line under same conditions if the VGT G/O turbine of CS 2 is chosen. Indeed, the VGT racks are usually more thermally robust than basic valves. Furthermore, the breakthrough result is the feasible end of correlation between BSFC and CO_2 emissions due to CO_2 capture. Also, forthcoming researches will be geared towards oxy-fuel combustion CFD studies and experimental campaign. Along with the testing, the CO_2 capture system will be coupled to the oxy-fuel combustion engine configurations depicted in this work. At last, assessment of the engine under partial load conditions with a physically-validated combustion model will be performed.

References

[1] E. Commission, 2030 climate and energy framework in European Union, https://ec.europa.eu/clima/policies/strategies/2030_en.

[2] E. Commission, A european strategy for low-emission mobility, https://ec.europa.eu/clima/policies/transport_en#tab-0-0.

[3] J. Galindo, J. Luján, J. Serrano, V. Dolz, G. Stéphane, Design of an exhaust manifold to improve transient performance of a high-speed turbocharged diesel engine, Experimental Thermal and Fluid Science - EXP THERM FLUID SCI 28 (2004) 863–875. doi:10.1016/j.expthermflusci.2004.01.003.

[4] F. Leach, G. Kalghatgi, R. Stone, P. Miles, The scope for improving the efficiency and environmental impact of internal combustion engines, Transportation Engineering 1 (2020) 100005. doi:10.1016/j.treng.2020.100005.

[5] J. Desantes, S. Molina, R. Novella, M. Lopez-Juarez, Comparative global warming impact and NO_x emissions of conventional and hydrogen automotive propulsion systems, Energy Conversion and Management 221 (2020) 113137. doi:10.1016/j.enconman.2020.113137.

[6] B. Metz, O. Davidson, P. Bosch, E. al, IPCC AR4. climate change 2007: Mitigation. contribution of working group iii to the fourth assessment report of the intergovernmental panel on climate change, Climate change 2007: The physical science basis 4.

[7] B. Buhre, L. Elliott, C. Sheng, R. Gupta, T. Wall, Oxy-fuel combustion technology for coal-fired power generation, Progress in Energy and Combustion Science 31 (2005) 283–307. doi:10.1016/j.pecs.2005.07.001.

[8] B. Abraham, J. Asbury, E. Lynch, A. Teotia, Coal-oxygen process provides CO_2 for enhanced recovery, Oil and Gas Journal 80.

[9] A. Simpson, A. Simon, Second law comparison of oxy-fuel combustion and post-combustion carbon dioxide separation, Energy Conversion and Management - ENERG CONV MANAGE 48 (2007) 3034–3045. doi:10.1016/j.enconman.2007.06.047.

[10] X. Pei, L. Yan, C. Wang, W. Song, J. Song, Process simulation of oxy-fuel combustion for a 300mw pulverized coal-fired power plant using Aspen Plus, Energy Conversion and Management 76 (2013) 581–587. doi:10.1016/j.enconman.2013.08.007.

[11] D. Hanak, D. Powell, V. Manovic, Techno-economic analysis of oxy-combustion coal-fired power plant with cryogenic oxygen storage, Applied Energy 191 (2017) 193–203. doi:10.1016/j.apenergy.2017.01.049.

[12] N. Kimura, K. Omata, T. Kiga, S. Takano, S. Shikisima, The characteristics of pulverized coal combustion in O_2/CO_2 mixtures for CO_2 recovery, Energy Conversion and Management 36 (1996) 805–808. doi:10.1016/0196-8904(95)00126-X.

[13] W. Sanz, H. Jericha, B. Bauer, E. Göttlich, Qualitative and quantitative comparison of two promising oxy-fuel power cycles for CO_2 capture, Journal of Engineering for Gas Turbines and Power-transactions of The Asme - J ENG GAS TURB POWER-T ASME 130. doi:10.1115/1.2800350.

[14] X. Wei, V. Manovic, D. Hanak, Techno-economic assessment of coal-or biomass-fired oxy-combustion power plants with supercritical carbon dioxide cycle, Energy Conversion and Management 221 (2020) 113143. doi:10.1016/j.enconman.2020.113143.

[15] O. Biyiklioğlu, M. Tat, Tribological assessment of NiCr, Al_2O_3/TiO_2 , and Cr_3C_2/NiCr coatings applied on a cylinder liner of a heavy-duty diesel engine, International Journal of Engine Research (2020) 146808742093016doi:10.1177/1468087420930164.

[16] A. Escudero, S. Espatolero, L. Romeo, Oxy-combustion power plant integration in an oil refinery to reduce CO_2 emissions, International Journal of Greenhouse Gas Control 45 (2016) 118–129. doi:10.1016/j.ijggc.2015.12.018.

[17] F. Carrasco Maldonado, R. Spörl, K. Fleiger, V. Hoenig, J. Maier, G. Scheffknecht, Oxy-fuel combustion technology for cement production - State of the art research and technology development, International Journal of Greenhouse Gas Control 45 (2016) 189–199. doi:10.1016/j.ijggc.2015.12.014.

[18] M. Pamminger, W. Buyu, C. Hall, R. Vojtech, T. Wallner, The impact of water injection and exhaust gas recirculation on combustion and emissions in a heavy-duty compression ignition engine operated on diesel and gasoline, International Journal of Engine Research 21 (2019) 146808741881529. doi:10.1177/1468087418815290.

[19] R. Mobasheri, S. Khabbaz, Modeling the effects of high egr rates in conjunction with optimum multiple injection techniques in a heavy duty DI diesel engine, SAE Technical Papers 1. doi:10.4271/2014-01-1124.

[20] A. Osman, Feasibility study of a novel combustion cycle involving oxygen and water, SAE Technical Papersdoi:10.4271/2009-01-2808.

[21] A. Van Blarigan, D. Kozarac, R. Seiser, R. Cattolica, J.-Y. Chen, R. Dibble, Experimental study of methane fuel oxycombustion in a spark-ignited engine, Journal of Energy Resources Technology 136 (2013) 012203. doi:10.1115/1.4024974.

[22] Z. Kang, S. Chen, Z. Wu, J. Deng, Z. Hu, L. Li, Simulation study of water injection strategy in improving cycle efficiency based on a novel compression ignition oxy-fuel combustion engine, SAE International Journal of Engines 11. doi:10.4271/2018-01-0894.

[23] D. J. Payri F., Motores de combustión interna alternativos, Reverté, 2011.

[24] D. T. Guide, Engine emission control, https://dieselnet.com/tech/engine_emission-control.php.

[25] R. Bilger, Z. Wu, Carbon capture for automobiles using internal combustion rankine cycle engines, Journal of Engineering for Gas Turbines and Power-transactions of The Asme - J ENG GAS TURB POWER-T ASME 131. doi:10.1115/1.3077657.

[26] Z. Wu, X. Yu, L. Fu, J. Deng, L. Li, Experimental study of the effect of water injection on the cycle performance of an internal-combustion rankine cycle engine, Proceedings of the Institution of Mechanical Engineers, Part D: Journal of Automobile Engineering 228 (2014) 580–588. doi:10.1177/0954407013511069.

[27] X. Yu, Z. Wu, L. Fu, J. Deng, Z. Hu, L. Li, Study of combustion characteristics of a quasi internal combustion rankine cycle engine, SAE Technical Papers 11. doi:10.4271/2013-01-2698.

[28] R. Mobasheri, A. Abdel, Z. Peng, X. Li, A numerical study of the effects of oxy-fuel combustion under homogeneous charge compression ignition, International Journal of Engine Researchdoi:10.1177/1468087421993359.

[29] A. Mohammed, J.-B. Masurier, A. Elkhazraji, B. Johansson, Oxy-fuel HCCI combustion in a CFR engine with carbon dioxide as a thermal buffer, in: SAE Technical Paper, 2019, p. 11. doi:10.4271/2019-24-0119.

[30] Z. Kang, Z. Wu, Z. Zhang, J. Deng, Z. Hu, L. Li, Study of the combustion characteristics of a HCCI engine coupled with oxy-fuel combustion mode, SAE International Journal of Engines 10. doi:10.4271/2017-01-0649.

[31] R. Mobasheri, N. Izza, A. Aitouche, J. Peng, B. Bakir, Investigation of oxyfuel combustion on engine performance and emissions in a DI diesel HCCI engine, in: International Conference on Systems and Control, 2019, pp. 411–416. doi:10.1109/ICSC47195.2019.8950525.

[32] T. Sharma, A. Rao, M. K, Homogeneous charge compression ignition (HCCI) engines: A review, Archives of Computational Methods in Engineering 23. doi:10.1007/s11831-015-9153-0.

[33] R. Mobasheri, A. Aitouche, Z. Peng, X. Li, Influence of oxy-fuel combustion on engine operating conditions and combustion characteristics in a high speed direct injection (hsdi) diesel engine under homogenous charge compression ignition (hcci) mode, in: SAE Technical Paper, WCX SAE World Congress Experience, 2020, p. 10. doi:10.4271/2020-01-1138.

[34] A. Mohammed, A. Elkhazraji, S. Jan, B. Johansson, A study on the performance and emissions of hcci oxy-fuel combustion in a cfr engine with recirculated carbon dioxide, in: SAE Powertrains, Fuels and Lubricants Meeting, 2020, p. 13. doi:10.4271/2020-01-2065.

[35] I. Mohsin, T. Al-Attas, K. Sumon, J. Bergerson, S. McCoy, M. Kibria, Economic and environmental assessment of integrated carbon capture and utilization, Cell Reports Physical Science 1 (2020) 100104. doi:10.1016/j.xcrp.2020.100104.

[36] O. Bushuyev, P. Luna, C. T. Dinh, L. Tao, G. Saur, J. Lagemaat, S. Kelley, E. Sargent, What should we make with CO_2 and how can we make it?, Joule 2. doi:10.1016/j.joule.2017.09.003.

[37] S. Sharma, F. Maréchal, Carbon dioxide capture from internal combustion engine exhaust using temperature swing adsorption, Frontiers in Energy Research 7 (2019) 143. doi:10.3389/fenrg.2019.00143.

[38] N. Mancini, A. Mitsos, Conceptual design and analysis of ITM oxy-combustion power cycles, Physical chemistry chemical physics : PCCP 13 (2011) 21351–61. doi:10.1039/c1cp23027a.

[39] C. N. del Medio Ambiente CONAMA 10, Captura y almacenamiento de CO_2, http://www.conama10.conama.org/conama10/download/files/GTs%202010/2_final.pdf.

[40] E. Portillo, B. Alonso-Fariñas, F. Vega, M. Cano, B. Navarrete, Alternatives for oxygen-selective membrane systems and their integration into the oxy-fuel combustion process: A review, Separation and Purification Technology 229 (2019) 115708. doi:10.1016/j.seppur.2019.115708.

[41] A. Leo, S. Liu, J. Costa, Development of mixed conducting membranes for clean coal energy delivery, International Journal of Greenhouse Gas Control 3 (2009) 357–367. doi:10.1016/j.ijggc.2008.11.003.

[42] S. Hashim, A. Mohamed, S. Bhatia, Oxygen separation from air using ceramic-based membrane technology for sustainable fuel production and power generation, Renewable and Sustainable Energy Reviews 15 (2011) 1284–1293. doi:10.1016/j.rser.2010.10.002.

[43] R. Kriegel, L. Kiesel, R. Kircheisen, U. Pippardt, Performance of various archetypes of oxygen membranes for local oxygen supply., in: DKG-Jahrestagung, 10. München, 2018, p. 10. doi:10.13140/RG.2.2.16996.83842.

[44] F. Wu, M. Argyle, P. Dellenback, M. Fan, Progress in O_2 separation for oxy-fuel combustion–a promising way for cost-effective CO_2 capture: A review, Progress in Energy and Combustion Science 67. doi:10.1016/j.pecs.2018.01.004.

[45] A. Arratibel, A. Labella, Y. Liu, N. Porras, D. Tanaka, M. Annaland, F. Gallucci, Mixed ionic-electronic conducting membranes (MIEC) for their application in membrane reactors: A review, Processes 7 (2019) 128. doi:10.3390/pr7030128.

[46] S. Baumann, J. Serra, M. Lobera, S. Escolástico, F. Schulze-Kuppers, W. Meulenberg, Ultrahigh oxygen permeation flux through supported $Ba_{0\cdot5}Sr_{0\cdot5}Co_{0\cdot8}Fe_{0\cdot2}O_{3-\delta}$ membranes, Journal of Membrane Science 377 (2011) 198–205. doi:10.1016/j.memsci.2011.04.050.

[47] D. Catalán Martínez, M. Santafé-Moros, J. Gozálvez-Zafrilla, J. García Fayos, J. Serra, Characterization of oxygen transport phenomena on BSCF membranes assisted by fluid dynamic simulations including surface exchange, Chemical Engineering Journal 387 (2020) 124069. doi:10.1016/j.cej.2020.124069.

[48] F. Arnau, J. Benajes, J. Desantes, J. Serrano, J. Serra, D. Catalán-Martínez, L. García-Cuevas, Motor de combustión interna de hidrocarburos auto transportable que no emite gases nocivos ni CO_2; secuestra CO_2 atmosférico y fabrica CO_2 líquido subcrítico, p201930285 (03 2019).

[49] J. Martín, F. Arnau, P. Piqueras, A. Auñón, Development of an integrated virtual engine model to simulate new standard testing cycles, SAE Technical Papers 2018-April. doi:10.4271/2018-01-1413.

[50] P. Olmeda, J. Martín, F. J. Arnau, S. Artham, Analysis of the energy balance during world harmonized light vehicles test cycle in warmed and cold conditions using a virtual engine, International Journal of Engine Research 21 (6) (2020) 1037–1054.

[51] F. Payri, F. Arnau, P. Piqueras, M. Ruiz, Lumped approach for flow-through and wall-flow monolithic reactors modelling for real-time automotive applications, in: SAE International, 2018. doi:10.4271/2018-01-0954.

[52] B. N.C., Fundamentals of turbocharging, Concepts NREC, 2005.

[53] G. D. Perry R., Perry's chemical engineers's handbook eighth edition, McGraw-Hill, 2008.

[54] S. of Automotive Engineers Inc., Turbocharger gas stand test code, Tech. Rep. J1826, SAE Standard (1995).